# PREPARATION AND CHARACTERIZATION OF ADSORBENT MATERIALS FROM TARO (*Colocasia esculenta*) PLANTS FOR THE REMOVAL OF ARSENIC IONS FROM CONTAMINATED WATER

**A DISSERTATION SUBMITTED FOR THE PARTIAL FULFILLMENT OF THE REQUIREMENTS FOR THE MASTER OF SCIENCE DEGREE IN CHEMISTRY**

BY

**Durgeshwar Prasad Sah**

**Exam Symbol No.: 2023/077**

Registration No.: 5-2-15-467-2016


**CENTRAL DEPARTMENT OF CHEMISTRY**

INSTITUTE OF SCIENCE AND TECHNOLOGY

TRIBHUVAN UNIVERSITY, KIRTIPUR, KATHMANDU, NEPAL

JULY 2025

## BOARD OF EXAMINERS AND CERTIFICATE OF APPROVAL

This dissertation entitled, **"Preparation and Characterization of Adsorbent Materials from Taro (*Colocasia esculenta*) Plants for the Removal of Arsenic Ions from Contaminated Water"**, by Durgeshwar Prasad Sah, under the supervision of Prof. Dr. Vinay Kumar Jha, Head of Department, Central Department of Chemistry, Tribhuvan University, Nepal, is hereby submitted for the partial fulfillment of the Master of Science (M.Sc.) Degree in Chemistry. This dissertation has not been submitted in any other university or institution previously for the award of a degree.

**……**

**Supervisor & Head of Department**
Prof. Dr. Vinay Kumar Jha,
Central Department of Chemistry
Tribhuvan University, Kirtipur
Kathmandu, Nepal

……
**External Examiner**
Dr. Manju Showree Karmacharya
Assistant Professor
Bhaktapur Multiple Campus
Bhaktapur, Nepal

……
**Internal Examiner**
Dr. Bhanu Bhakta Neupane
Assistant Professor
Central Department of Chemistry
Tribhuvan University, Kirtipur
Kathmandu, Nepal

**Date: July 28, 2025**

## RECOMMENDATION

This is to certify that the dissertation entitled, **"Preparation and Characterization of Adsorbent Materials from Taro (*Colocasia esculenta*) Plants for the Removal of Arsenic Ions from Contaminated Water"** has been carried out by Durgeshwar Prasad Sah as a partial fulfillment for the requirements of M. Sc. Degree in Chemistry under my supervision. To the best of my knowledge, this work has not been submitted or published to any other degree in this institute or any other institutions or University.

---

**Supervisor & Head of Department**

Prof. Dr. Vinay Kumar Jha

Central Department of Chemistry

Tribhuvan University, Kirtipur, Kathmandu, Nepal

**July 28, 2025**

## DECLERATION

I, **Durgeshwar Prasad Sah**, hereby declare that the work presented herein is genuine work done originally by me and has not been published or submitted elsewhere for the requirement of a degree program. Any literature, data or works done by others and cited in this dissertation has been given due acknowledgement and listed in the reference section.

…….

Durgeshwar Prasad Sah
Exam Symbol No.: 2023/077
T.U. Regd. No.: 5-2-15-467-2016
Central Department of Chemistry
Tribhuvan University, Kirtipur, Kathmandu, Nepal

## DEDICATION

I sincerely dedicate this thesis to my beloved parents, **Mr. Sonalal Sah** and **Mrs. Shivkumari Devi**, whose unconditional love, constant support, and immense sacrifices have been the foundation of my life and learning. Their encouragement, patience, and unwavering belief in me have been the greatest source of strength throughout my academic journey. This achievement would not have been possible without their guidance and blessings.

## ACKNOWLEDEMENTS

I would like to express my deepest gratitude to all those who have supported and guided me throughout the process of completing this thesis.

First and foremost, I am sincerely thankful to my supervisor Prof. Dr. Vinay Kumar Jha, who is fortunately and co-incidentally the current Head of Department of Central Department of Chemistry (CDC), TU for his invaluable guidance, continuous encouragement, and constructive feedback throughout my research.

I prompt my profound appreciativeness to Prof. Dr. Jagadeesh Bhattarai, the former Head of the Department, CDC, for giving me the necessary physical conveniences to conduct this study.

I am grateful to all faculty members Asst. Prof. Dr. Bhanu Bhakta Neupane, Asst. Prof. Dr. Santosh Khanal, Asst. Prof. Dr. Hari Poudel, guests and all the staff of CDC.

I am extremely grateful to Nepal Academy of Science and Technology (NAST) for XRD and FTIR. Similarly, I would like to thanks Assit. Prof. Dr. Sabita Shrestha, CDC for for FTIR. Special thanks to my colleagues and friends, Shankar Kunwar, Shree Krishna Shah Teli, for their support, helpful discussions, and encouragement.

I am grateful to the Central Department of Chemistry (CDC) for providing the necessary resources and a conductive environment for my research.

Finally, I would like to thank my Parents and family for their unconditional love, patience, and support throughout this journey.

## LIST OF ABBREVIATIONS AND SYMBOLS

AC→ Activated Carbon

ACL→ Activated Colocasia Leave

ACR→ Activated Colocasia Root

ACS→ Activated Colocasia Stalk

DCLP→ Dried Colocasia Leaves Powder

DCRP→ Dried Colocasia Roots Powder

DCSP→ Dried Colocasia Stalks Powder

FTIR→ Fourier Transform Infrared Spectroscopy

MB→ Methylene Blue

OM→ Optical Microscopy

SSA→ Specific Surface Area

XRD→ X-ray Diffraction

## ABSTRACT

Arsenic contamination in drinking water remains a critical global health issue, necessitating the development of effective and sustainable remediation technologies. This research investigates the preparation and characterization of adsorbent materials derived from Taro (*Colocasia esculenta*) plants for the removal of arsenic ions from contaminated water. Dried Colocasia Powder (DCP) was chemically activated and ground into a fine powder. The prepared biochar was subjected to comprehensive characterization using techniques such as X-ray Diffraction (XRD), Fourier Transform Infrared Spectroscopy (FTIR), and methylene blue adsorption method. The FTIR analysis revealed the presence of functional groups such as hydroxyl, carboxyl, and alkene. The crystal planes of the XRD analysis are showed mostly amorphous nature of the adsorbents. The specific surface area values for ACR, ACS, and ACL were 448, 502, and, 478 $m^2/g$, respectively. With a high specific surface area, activated *Colocasia* stalk (ACS) was shown to be the best adsorbent among the three. The adsorption of As(III) was pH dependent and maximum at 7. The equilibrium time for adsorption of As(III) on ACS was less than 50 minutes. The adsorption data followed pseudo-second order kinetics with rate constant 0.01830 g/mg.min. The equilibrium adsorption capacity was determined from Langmuir model and was found to be 62.5 mg/g. Desorption and regeneration studies revealed that the biochar adsorbents retained significant reusability, maintaining over 85% of their initial arsenic removal efficiency after three cycles.



***Keywords:*** Biochar; Chemisorptions; Methylene Blue; Reflux; Taro.

## शोधसार

पिउने पानीमा आर्सेनिक प्रदुषण अझै एक गम्भीर विश्वव्यापी स्वास्थ्य समस्याको रुपमा रहेको छ, जसको सामाधानका लागि प्रभावकारी र दिगो प्रविधिको विकास आवश्यक छ । यस अनुसन्धानमा पिडाँलुको विभिन्न भागहरुबाट तयार पारिएको अवशोषकहरुका तयारी र विशेषताहरुको अध्ययन गरिएको छ, जसको प्रयोग आर्सेनिकयुक्त दुषित पानीबाट As(III) लाई हटाउनका लागि प्रयोगको अध्ययन गरिएको हो । सुकाइएको पिँडालुको पाउडरलाई रासायनिक रुपमा सक्रिय बनाई, ससाना कणहरुमा पीसिएको थियो । तयार पारिएको बायोचारहरुको विशेषता पत्ता लगाउन X-ray Diffraction, FTIR, र Methylene blue अवशोषण विधिको प्रयोग गरियो । FTIR विश्लेषणले हाइड्रोक्सिल, कार्बोक्सिल, र अल्किन जस्ता कार्यात्मक समूहहरुको उपस्थिति देखाएको छ । XRD विश्लेषणले पिँडालुको सक्रिय जरा, डाँठ र पातहरु धुलो ठोस भएको देखायो । पिँडालुको सक्रिय जरा, डाँठ र पातबाट बनेका अवशोषकहरुको विशिष्ट सतहको क्षेत्रफल क्रमश: ४४८, ५०२ र ४७८ वर्ग मिटर प्रति ग्राम रहेको पाइयो । ती मध्ये पिँडालुको सक्रिय डाँठ को विशिष्ट सतहको क्षेत्रफल सबैभन्दा बढी देखिएको हुनाले यो सबैभन्दा प्रभावकारी अवशोषक भएको पाइयो । pH ७ मा As(III) को अवशोषण अधिकतम भएको पाइयो । As(III) को Adsorption Equilibrium Time ५० मिनेट भन्दा कम थियो । अवशोषण डाटा pseudo-second order kinetics लाई पछ्याउने देखियो जसको rate constant ०.०१८३ ग्राम प्रति किलोग्राम.मिनट दायरामा थियो । Langmuir model अनुसार As(III) को सन्तुलन अवशोषण क्षमता ६२.५ मिलिग्राम प्रति ग्राम रहेको पत्ता लगाइयो । डिसर्पसन र रिजेनेरेसन अध्ययनहरुले देखाए अनुसार, बायोचार एडसर्बेन्टहरुले तीन चक्रसम्म प्रयोग गरेपछि पनि आफ्नो सुरुको आर्सेनिक हटाउने क्षमता ८५ % भन्दा बढि कायम राखेको थियो, जसले ती सामग्रीहरुलाई पुन: प्रयोग गर्न मिल्ने दिगो सामाधानको रुपमा प्रमाणित गर्छ ।



***शब्दकुञ्जी*** : केमिजर्पसन; पिडाँलु; बायोचार; मिथाइलिन ब्लु; रिफ्लक्स ।

## TABLE OF CONTENTS

## LIST OF FIGURES

## LIST OF TABLES

# CHAPTER 1: INTRODUCTION

## 1.1 General Introduction

Water is becoming more and more contaminated day by day. Water pollution is defined as any chemical, biological, or physical change to the quality of water that endangers living things or renders the water unfit for intended purposes. Sewage and other wastes requiring oxygen, infectious agents, plant nutrients, unusual organic chemicals, inorganic mineral and chemical compounds, sediments, radioactive materials, thermal pollution oils, and detergents are just a few of the pollutants that can contaminate water (Feng et al., 2011). It is a significant environmental issue that contemporary society faces, one that poses risks to human health and ecological equilibrium. Acute toxicity is present for both aquatic and terrestrial species, including people, when exposed to heavy metal ions like copper, cadmium, lead, nickel, and chromium, which are frequently detected in waste water from factory. Therefore, releasing effluents into the environment is a major worry (Matlock et al., 2002).

The functions and chemical properties of the heterogeneous group of elements known as heavy metals vary. In the Periodic Table, heavy metals primarily belong to the transition element. Elements with a specific weight of greater than 5 $g.cm^{-3}$ are classified as heavy metals (Leonard et al., 2004). It gets into the aquatic ecosystem through air deposition, mining wastes, anthropogenic activities resulting in industrial effluents, erosion of the geological matrix, and domestic sewage (Baby et al., 2011). Potential biosorbent such as biomass of algae, aquatic ferns, and seaweeds, waste biomass derived from plants, mycelia wastes from fermentation businesses, etc., were utilized to remove heavy metals from aqueous solutions and waste water (Ahluwalia & Goyal, 2007).

Arsenic (As) based contaminants is a major issue for current ground-water-based drinking water delivery system of Nepal, and it is now recognized as being one of the most urgent environmental health management challenges, particularly in Terai districts where the population is dependent on hand tubes and wells that have been dug for their everyday consumption of water. The low amount of arsenic contamination was recorded in the districts of Ilam, Morang, Jhapa, Udaypur, Mahottari, Kathmandu, Lalitpur, Parsa, Bara, Dang, and Bardiya, Palpa, Chitwan.

There was arsenic contamination in the area of Sunsari, Saptari, Siraha, Dhanusha, Sarlahi, Rauthat, Bara, Nawalparasi, Rupandehi, Kapilbastu, Banke, Kailali, and Kanchanpur that ranged from 10 to 50 g/L and even higher (Thakur et al., 2010).

**Arsenic**

The naturally occurring steel gray metalloid arsenic (VA element) has an atomic weight of 74.92 g/mol. and an atomic number of 33. It is symbolized by the symbol As. Arsenic is typically found in two forms: inorganic and organic. There are various oxidation states of arsenic found in the environment, including -3, 0, +3 and +5. Trivalent arsenite or pentavalent arsenate forms of inorganic arsenic are typically encountered in aqueous solutions (Babaee et al., 2018).

Pentavalent species are:

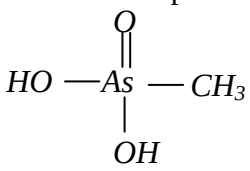

**Monomethylarsonic Acid**

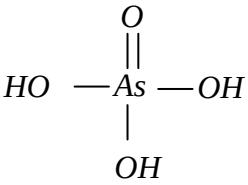

**Arsenic Acid**

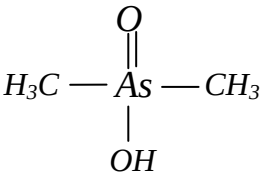

**Dimethylarsinic Acid**

Trivalent species are;

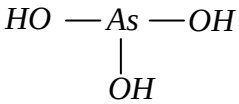

**Arsenious Acid, Arsenite**

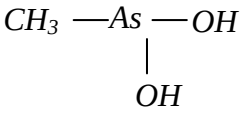

**Monomethylarsonous Acid**

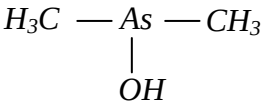

**Dimethylarsinous Acid**

Whereas arsenite maintains in anaerobic water under reducing circumstances, arsenate prevails in drinking water under oxidizing conditions. Inorganic arsenic is formed when arsenic is coupled with elements like oxygen, chlorine, and sulfur; organic arsenic is formed when arsenic is combined with carbon and hydrogen (Karmacharya et al., 2016). +3 and +5 oxidation states are frequently observed in water systems, depending on the prevailing redox circumstances; elemental states like -3 and 0 are extremely rare. While several hydrolysis species of As(V), such as $H_3AsO_4$, $H_3AsO_4^-$, $HAsO_4^{2-}$, can be present in water with dissolved oxygen or an oxidizing environment, As (III) is primarily found as $H_3AsO_3$, $H_2AsO_3^-$, $HAsO_3^{2-}$, and $AsO_3^{3-}$ under reducing environments (Pant et al., 2012). As (III) is more toxic and mobile (Gulens & Anson, 2002; Morrison et al., 1990) than the As(V) that are found in water and is present in

reducing conditions (Kuriakose et al., 2004). Numerous acute and chronic illnesses have been documented, including diarrhea, stomach pain, and nausea. The National Research Council (NRC) states that exposure to arsenic over a long period of time can result in skin lesions as well as cancers of the bladder, lungs, skin, kidneys, liver, and prostate. Drinking water with a high arsenic content has been linked to nearly identical side effects, including multisystem dysfunction and the deactivation of enzymes involved in DNA synthesis and repair (Ratnaike, 2003).

Considering these complications, a global overview of National regulation and standards for drinking water quality has recommended the WHO guideline value for arsenic which is 0.01 mg/L (World Health Organization, 2018), and at the same time the government of Nepal, National Drinking Water Quality Standards, 2062 has launched the concentration limit which is 0.05 mg/L (Gnawali et al., 2023). Therefore, effective methods for the removal of arsenic ions from contaminated water are of utmost importance.

For designing adsorption process, suitable, easily available, accessible, and cost-effective adsorbent materials should be required. One of the most explored adsorbent materials from ancient times is activated carbon (AC). Activated carbon is a type of microporous carbon that has a large internal surface area, well-developed pore structure, and pore volume. As a result, it has a high adsorption capacity. Additionally, the AC has functional groups on its surface that affect the pH of the solution and, in turn, the adsorption procedure (Jjagwe et al., 2021). Due to its wide porous structure, large surface area, high capacity, and hydrophobic character, commercial activated carbon (CAC) is most frequently utilized in the water and wastewater treatment industries. However, coal-based CAC is expensive and has serious regeneration problems because it is mainly obtained from non-renewable sources such as coal, lignite, and peat (Sen, 2023). When compared to commercially produce adsorbent materials, those made from readily available agricultural biowaste appear to be more affordable and available to the local populations. Micropores can be created on plant-based adsorbent materials, which are readily available and affordable, with the right activation technique (Jha & Jha, 2021). As a result, current research is concentrating on the use of various carbonaceous, lignocellulosic, and agricultural byproduct solid wastes, such as fruit and vegetable wastes, leaves, seeds,

tree waste, fibers, fruit peels, dates, sawdust, bark, etc., for the creation of a successful adsorbent alternative to pricey coal-based activated carbon (Sen, 2023).

**Removal Strategies of Arsenic**

Ion exchange, membrane filtration, reverse osmosis, chemical precipitation, and adsorption are a few techniques that have been described in the past for removing $As^{3+}$ and $As^{5+}$ from aqueous solutions. Adsorption-based separation technique is one of the most efficient but often used methods of treating wastewater and water contaminated with heavy metals. It is a form of sustainable development because of its straightforward operation, straightforward design, high separation efficiency, efficiency at lower pollutant concentrations, high molecular selectivity, low energy consumption, and capacity to separate multiple pollutant components with little secondary pollution (Sen, 2023). By utilizing adsorption process, even low concentrations of arsenic ions such as 1.0 mg/L can be removed (Wilde & Benemann, 1993).

**Taro (*Colocasia esculenta*) and its Uses**

Taro (*Colocasia esculenta*) plant shown in **Figure 1.1**, an Araceae family member, is an ancient crop used across the humid tropics for its delicious corms and leaves, as well as for traditional ceremonial purposes. The plant is said to have expanded from India, where it is thought to have originated, eastward through Burma and China, and southward to Indonesia (Wang & Higa, 1983). A study reported that taro plants contain about 62-76% carbohydrates, protein in between 13 to 25%, fibers 1-2%, calcium from 0.29 to 0.72%, and iron from 0.18 to 1.18 mg/100g. Calcium and iron contents in these plants are expected to favor the adsorption of arsenic ions (Boampong et al., 2019).

The choice of raw materials is crucial in the preparation of AC. The characteristic of AC is significantly influenced by the nature of the raw material. Materials are chosen depending on their accessibility, availability, purity, and degree of activation (Ahmed & Theydan, 2012). One of the most important ways to increase the adsorbent's adsorption efficiency is to improve adsorption by using inexpensive adsorbent materials, such as readily available agricultural waste, and physico-chemically modifying them to introduce surface functional groups. Thus, in this work, arsenic

ions are cured from aqueous solution utilizing acid activated carbon generated from powdered Taro plants.


***Fig. 1.1**: (a) Corms, (b) stalk, and (c) leaves of taro plants*

### 1.2 Methods for the Determination of Specific Surface Area

The Specific Surface area (SSA) is defined as the ratio of the total surface area to the total mass of adsorbent materials. It is measured in $m^2/g$. Pyrolysis temperature, heating, and type of feedstock are the main factors that have huge effect on surface area resulting in values ranging from 10 to $10^3$ $m^2/g$ (Kundu et al., 2023). Specific surface area of adsorbent is generally determined by following techniques:

a. Branauer-Emmett-Teller Method (BET Method)
b. Iodine Number Method
c. Methylene Blue Adsorption Method (MBAM)

The multilayer adsorption of gaseous molecules (such as oxygen, nitrogen, argon, or methane) on the adsorbent surface occurs in conjunction with the BET technique. Although the experimental setup is time-consuming and the approach is quite accurate, it requires specialized knowledge and advanced instruments that are not yet available in our nation. Furthermore, "capillary condensation" renders the BET theory unreliable at greater relative vapor pressures. Because $N_2$ cannot pass through intermolecular gaps or micropores, polar adsorbates like EGME and $H_2O$ provide a larger estimate of specific surface area than non-polar compounds like $N_2$ (Jong, 1999).

One of the techniques frequently used in the industry with activated carbon is the measurement of the iodine number. The adsorption of iodine on the oxidized active carbons was specifically examined using this technique. It is important to remember that the iodine number method's surface properties have few physical meanings. The process in many microporous systems is best explained by the mechanism of micropore volume filling rather than surface covering. Therefore, for such adsorption

systems exhibiting low dependability, specific surface areas cannot have any physical importance (Mianowski et al., 2007).

The methylene blue adsorption method was frequently used to determine specific surface area for a variety of natural solids, including silica, graphite, charcoal, and activated carbon. This approach is straightforward, quick, easy, dependable, and affordable. This technique is simple to use in any laboratory. This approach uses the Langmuir adsorption isotherm to calculate the specific surface area when a constant amount of adsorbent is added to various concentrations of MB solution. The specific surface area is determined by MBAM in which it is assumed that MB adheres in a monolayer to the surface of the sorbent particle.

$$S_{MB} = \frac{Q_{MAX} \cdot a_{MB} \cdot N}{M_{MB}} \ldots\ldots\ldots (1.1)$$

Where, $S_{MB}$ is the specific surface area in $m^2/g$, $Q_{max}$ is the mass in gram of methylene blue adsorbed per gram of sorbent, $a_{MB}$ is the area occupied by one molecule of methylene blue in $m^2$/molecule, N is the Avogadro's number ($6.023\times10^{23}$ molecules/mol) and $M_{MB}$ is the methylene blue molar mass i.e. 373.9 g/mol (Goourlot et al., 1998).

### 1.3 Methods for the Determination of As(III) ion

Numerous techniques for determining the concentration of arsenic in an aqueous system have been developed. Some of these techniques are inexpensive and quick, others are expensive and time-consuming. The following list includes the several analytical techniques used to determine arsenic:

(i) Field kit method (Giles et al., 2011)
(ii) Molybdenum blue method (Anzai et al., 2011)
(iii) Atomic Fluorescence Spectroscopy (Gallardo et al., 2001)
(iv) Inductively coupled plasma mass spectroscopy (ICP-MS) (Heitkemper et al., 2001)
(v) Hydride generation atomic absorption spectroscopy (HGAAS) (Muñoz et al., 1999)
(vi) Atomic absorption spectroscopy (Aggett & Aspell, 1976)
(vii) Square wave cathodic stripping voltammetry (SWCSV) at a hanging mercury drop electrode (HMDE) (Ferreira & Barros, 2002)

(viii) Inductively coupled plasma atomic emission optical emission spectroscopy (ICP AEOES)

(ix) Graphite furnace atomic absorption spectrometry (GFAAS)

(x) Silver diethyl dithiocarbamate spectrophotometric method (SDDC) (Aggett & Aspell, 1976)

Despite being the best techniques, ICP-MS and ICP-AES are not the preferred procedures for institutions with poor laboratory conditions due to their high cost and lack of access to such advanced equipments. The SWCSV techniques shown a strong association with optical emission spectroscopy with ICP connected to hydride production however using it in our labs is also challenging. The Gulzeit and Silver diethyl dithiocarbamate methods are not cost-effective, but atomic absorption spectroscopy seemed to be the most suitable in terms of sensitivity and precision at low levels and is more compatible with a quick arsine production process (Aggett & Aspell, 1976). The molybdenum blue method, which was used by a number of researchers in the past, is still the preferred technique for determining As(III) due to its simplicity, affordability, speed, precision, and accuracy.

## 1.4 Adsorption Studies

### 1.4.1 Adsorption isotherms

The most often used models for determining different adsorption parameters in aqueous solutions and studying the predominant adsorption mechanisms are the Freundlich and Langmuir models (Babaee et al., 2018).

**Langmuir adsorption isotherm**

The Langmuir adsorption isotherm, which was proposed by Langmuir in 1918, is a relationship between the concentration and the amount adsorbed for a unimolecular layer. Langmuir assumed that there was no interaction between the adsorbed molecules and that the adsorbent molecules had monolayer surface coverage with energetically equal adsorption sites (Langmuir, 1918).

Equation (1.2) represents the general Langmuir's adsorption isotherm:

$$Q_e \left(= \frac{X}{M}\right) = \frac{bQ_{max}\, C_e}{1 + bC_E} \ldots\ldots\ldots (1.2)$$

Where

$Q_e$ = equilibrium adsorption capacity (mg/g),

X = mass of adsorbate (mg),

M = mass of adsorbent (g),

$Q_{max}$ = maximum adsorption capacity (mg/g),

b = constant related to adsorption energy (L/mg), and

$C_e$ = equilibrium concentration of the ions adsorbed (mg/L).

Equation (1.3) is the linearized form of equation (1.2):

$$\frac{C_e}{Q_e} = \frac{1}{Q_{max}\, b} + \frac{C_e}{Q_{max}} \ldots\ldots\ldots\ldots (1.3)$$

Thus, when a graph is plotted between $\frac{C_e}{Q_e}$ as ordinate and $C_e$ as abscissa, a straight line is obtained whose slope will be equal to $\frac{1}{Q_{max}}$ and intercept gives the value of $\frac{1}{Q_{max}\, b}$ . Here, $Q_{max}$ and b are determined using slope and intercept, respectively. The dimensionless separation factor $(K_L)$, characterizes the type of isotherm, can be used to explain the key features of the Langmuir isotherm.

$$K_L = \frac{1}{1 + bC_i} \ldots\ldots\ldots\ldots (1.4)$$

Where,

$C_i$ = initial concentration of the adsorbate in mg/L, and

$K_L$ = Langmuir equilibrium parameter.

$K_L$ Indicates the shape of isotherms and the type of adsorption process [$K_L > 1$, unfavorable, $K_L = 1$, linear,$0 < K_L < 1$, favorable, $K_L = 0$, irreversible]. Therefore, $K_L$ the value should fall between 0 and 1 for favorable isotherms.

**Freundlich adsorption isotherm**

An empirical equation known as the Freundlich adsorption isotherm was established by Freundlich in 1909 to depict the adsorption relationship generally. Freundlich suggests that a heterogeneous adsorbent surface with an uneven heat of adsorption (Freundlich & Heller, 1939). It is written as,

$$Q_e = K_F C_e^{\frac{1}{n}} \ldots\ldots\ldots (1.5)$$

where $K_F$ and n are Freundlich isotherm constants that correspond to the adsorption intensity and adsorption capacity, respectively. On taking logarithms on both sides of equation (1.5), we get equation (1.6):

$$\log Q_e = \log K_F + \frac{1}{n}\log C_e \ldots\ldots\ldots\ldots (1.6)$$

When a graph is plotted between $\log Q_e$ as ordinate and $\log C_e$ as abscissa, intercept gives the value of $K_F$ and slope gives the value of n.

### 1.4.2 Adsorption kinetics

The equilibration time and adsorption rate of target metal ions on the chemically modified adsorbent surface are ascertained by kinetic tests. The mechanism of solute adsorption onto an adsorbent can also be expressed using kinetic experiments that describe many models. To examine the reaction kinetics, several adsorption kinetic models have been proposed. The two most commonly utilized models among them are pseudo-first order and pseudo-second order kinetic models. The adsorption mechanism of the metal ions on the adsorbent surface, when correlation coefficient values are challenging to interpret, can also be described by the adsorption capacity (Schiewer & Balaria, 2009).

**Pseudo-first order kinetic model**

According to pseudo-first order kinetic model the rate of adsorption $\left(\frac{dQ}{dt}\right)$ at any time is directly proportional to the amount of surface unoccupied (i.e. $Q_e - Q_t$). The differential form of pseudo-first order rate equation (Lagergren, 1898) is given by:

$$\frac{dQ}{dt} = K_1(Q_e - Q_t) \ldots\ldots\ldots (1.7)$$

Where, $Q_e$ and $Q_t$ are the amounts of adsorbate adsorbed per unit weight (mg/g) of adsorbent at equilibrium and at time (t), respectively and $K_1$ ($min^{-1}$) is the first order Lagergren adsorption rate constant.

Linearized form of equation obtained by integrating equation (1.7) for the boundary conditions t = 0 to t = t and Qt = 0 to $Q_t = Q_e$ be given as:

$$\log(Q_e - Q_t) = \log Q_e - \frac{K_1}{2.303} \times t \ldots\ldots\ldots (1.8)$$

Hence, $Q_e$ and $K_1$ can be calculated from slope and intercept of graph plotted between $\log(Q_e - Q_t)$ and time.

**Pseudo-second order kinetic model:**

According to the pseudo-second order kinetic model, the rate of adsorption at any given time $\left(\frac{dQ}{dt}\right)$ is exactly proportional to the square of the number of vacant surface sites that are still available [i.e. $(Q_e - Q_t)^2$] (Ho & McKay, 1999). Therefore, the kinetic rate law can be generally expressed as follows:

$$\frac{dQ}{dt} = k_2(Q_e - Q_t)^2 \dots\dots\dots (1.9)$$

Where,

$Q_e$ = amount of adsorbate adsorbed per unit weight of adsorbent (mg/g) at equilibrium

$Q_t$ = amount of adsorbate adsorbed per unit weight of adsorbent (mg/g) at time (t),

$K_1$ = pseudo second order adsorption rate constant ($g \cdot mg^{-1} \cdot min^{-1}$).

On integrating and rearranging equation (1.9) for the boundary conditions t = 0 to t and $Q_t$ = 0 to $Q_t$ we get linearized equation for pseudo-second order reaction:

$$\frac{t}{Q_t} = \frac{1}{K_2 Q_e^2} + \frac{t}{Q_e} \dots\dots\dots (1.10)$$

Where, h $(= K_2 Q_e^2)$ is the initial adsorption rate ($mg \cdot g^{-1} \cdot min^{-1}$) and t is contact time. Hence, $K_2$ and $Q_e$ values can be calculated from slope and intercept of graph plotted between $\left(\frac{t}{Q_t}\right)$ and t.

### 1.5 Intraparticle Diffusion Model

The process describing the rate-determining step is identified by Weber and Morris intraparticle diffusion model (Campos et al., 2018).The general form of equation is expressed in the following equation:

$$Q_t = K_{id} dt^{0.5} + c \dots\dots\dots (1.11)$$

The intraparticle diffusion rate constant is $k_{id}$ ($mg/g.h^{\mathbf{0.5}}$), and C can be figured out from the slope and intercept of the curve drawn between $Q_t$ and $t^{\mathbf{0.5}}$. The boundary layer effect is described by the intercept of plot. An increase in the intercept of the plot indicates a greater contribution from surface adsorption in the rate-controlling phase. The intraparticle diffusion model is best described if $Q_t$ passes through the origin and changes linearly with $t^{0.5}$. The mechanism of intraparticle diffusion is not just the rate-limiting step of the adsorption process, as indicated if the entire plot does

not pass through the origin. The numerous linear segments of the plot show that other interaction mechanisms are at play (Nikić et al., 2019).

### 1.6 Thermodynamic Studies

The viability of the adsorption process is determined through thermodynamic investigations. The spontaneity of a chemical reaction is indicated by the change in Gibb's free energy ($\Delta G^o$). To determine the change in free energy ($\Delta G^o$), the thermodynamic equilibrium constant, also known as the thermodynamic distribution coefficient ($K_D$), is computed. The following generic phrase is used to calculate $K_D$:

$$K_D = \frac{a_s}{a_e} = \frac{V_s Q_e}{V_e C_e} \dots\dots\dots (1.12)$$

Where, $Q_e$ and $V_e$ represent the activity and activity coefficient of the adsorbate ions in solution at equilibrium, while $a_s$ and $V_s$ represent the activity and activity coefficient of the adsorbate ions adsorbed on the adsorbent surface. As a result, at infinite solution dilution, the activity coefficient tends to unity, meaning that $V_s = V_e = 1$. Hence:

$$\lim_{Q_e \to 0} \left(\frac{a_s}{a_e}\right) = \frac{1 \times Q_e}{1 \times C_e} = K_D \dots\dots\dots (1.13)$$

When the curve displayed between $ln\frac{Q_e}{C_e}$ versus $Q_e$ is extrapolated to zero, $K_D$ is determined by its intercept. The obtained value of $K_D$ is used to calculate the change in adsorption free energy ($\Delta G^o$), and this value is provided by:

$$\Delta G^o = -RTlnK_D \dots\dots\dots (1.14)$$

Importantly, rather than using the thermodynamic equilibrium constant $K_D$, ($\Delta G^o$) (kJ $mol^{-1}$) can be computed directly using the Langmuir constant b (Karmacharya et al., 2016).

$$\Delta G = -RTlnb \dots\dots\dots (1.15)$$

Where

R = the universal gas constant (8.314 J/mol.K),

T = temperature in Kelvin, and

b = the Langmuir constant in (L/mol.).

An energetically beneficial adsorption process is indicated by a negative value for Gibb's free energy,($\Delta G$). For physisorption process, its value falls between -20 and 0 $kJ.mol^{-1}$, whereas for chemisorption process, it falls between -80 and -400 kJ. $mol^{-1}$.

## 1.7 Literature Survey

A study shows arsenic contamination in drinking water is a serious global environmental issue, especially in South Asia, including Nepal, India, and Bangladesh. Naturally occurring arsenic leaches into groundwater from arsenic-rich geological formations, leading to chronic human exposure (Smedley & Kinniburgh, 2002).

A study of WHO shows long-term ingestion of arsenic-contaminated water can lead to various health problems, including skin lesions, cancer, and cardiovascular diseases (WHO, 2017). In many rural areas, especially in the Terai region of Nepal, groundwater is the primary source of drinking water, making arsenic contamination a public health concern.

A study on removal of arsenic shows various physical, chemical, and biological techniques have been developed to remove arsenic from water. These include coagulation-flocculation, ion exchange, membrane filtration, and adsorption (Mohan & Pittman, 2007). Among them, adsorption is considered one of the most effective and economical techniques due to its simplicity, low cost, and high efficiency. Activated carbon, metal oxides, and agricultural waste-derived adsorbents are commonly studied for this purpose (Gupta & Ali, 2004).

A study on water remediation shows using plant-derived biomass as low-cost adsorbents is a promising strategy for water remediation. Agricultural wastes and plant materials (peels, husks, leaves, etc.) are abundant, renewable, and often rich in cellulose, lignin, proteins and other biopolymers with functional groups that bind metals (Yeo et al., 2021).

A study on different activation process shows arsenic adsorption by plant-based adsorbents generally involves a combination of physical and chemical processes. Mechanisms include electrostatic attraction between As anions and positively charged surface sites, ligand exchange/completion with surface –OH/–$NH_2$ groups, and precipitation of insoluble arsenates (especially on iron-rich surfaces) (Banerjee et al., 2016).

A study on removal of arsenate demonstrates that untreated taro stem (biosorbent) removed about 58.6% of arsenate ($As^{5+}$) under optimal conditions (Maity et al., 2021).

This raw stem biomass showed Langmuir adsorption behavior and also followed pseudo-second-order kinetics, suggesting chemical interactions dominate its uptake.

A study reported that planted taro obtained in constructed wetland removed 89% of arsenic via root accumulation and iron-layer adsorption (Thathong et al., 2019). This highlights inherent affinity of *C. esculenta* for arsenic and underscores its potential both as a living plant and as a processed adsorbent.

A study on removal of arsenic from activated carbon obtained from jute sticks showed equilibrium adsorption efficiency as 80% (When initial As(III) concentration was 0.08 ppm) with a flow rate of 15 mL/min. Even with a very high concentration of arsenic solution (0.4 ppm), 100% arsenic removal was obtained when the solution was prepared with $KMnO_4$. Due to its neutral charge, As(III) exhibited physical adsorption on activated carbon. However, As(V) was efficiently adsorbed on the activated carbon due to its charge (Jahan et al., 2008).

A study for arsenic and chromium removal from water using bio chars derived from rice husk, organic solid wastes and sewage sludge showed the maximum adsorption efficiency of 25, 53, 55 and 65% for As(V) on bio char produced from rice-husk (BC-RH), bio char produced from sewage sludge (BC-SS), bio char produced from solid waste (BC-SW) and soil respectively at initial metal concentration of 90 $\mu g.L^{-1}$. The adsorption process was well fitted to Freundlich adsorption isotherm. Further, the adsorption processes were followed by pseudo-second-order kinetics with the rate constants in the range of 0.02 to 0.21 $h^{-1}$ for As(V) on different adsorbents (Agrafioti et al., 2014).

A study for effective removal of arsenic with Lanthanum(III) and Cerium(III)-loaded orange waste gels showed the equilibrium adsorption capacities of 43 mg/g and 42 mg/g for As(III) and As(V) respectively. As(V) and As(III) were completely retained on the gel up to 120 bed volumes (BV) for As(V) and 100 BV for As(III), while complete saturation was achieved at 690 and 280 BV, respectively (Biswas, Inoue, Ghimire, et al., 2008).

A study for the adsorption of arsenic ions from the adsorbent obtained from spinach leaves showed the maximum specific surface area as 490 $m^2/g$. The adsorption capabilities for As(III) was determined as 58.48 mg/g (Jha & Jha, 2021).

A study on the adsorption of arsenic ion from the activated carbon adsorbent obtained from Lapsi seeds has shown to be decreased the concentration of arsenic in water from 800 ppb to below 50 ppb (Rajbhandari et al., 1970).

A study for removal of As(III) from aqueous solution by biosorption on to maize (*Zea mays*) leaves surface showed the maximum adsorption efficiency of 84.98%. The Freundlich adsorption isotherm was fitted well to the adsorption data. Further, the adsorption of As(III) on maize leaf surface followed pseudo-second-order kinetics with the rate constant in the range of 0.321 g/mg. min (Kamsonlian et al., 2011).

A study for the removal of As(III) and As(V) using rubber tire derived activated carbon modified with alumina composites showed the equilibrium adsorption capacities of 14.28 and 23.80 mg/g for As(III) and As(V) respectively (Karmacharya et al., 2016).

A study for the removal of As(III) from aqueous solution using $Fe^{3+}$ loaded phosphorylated *Dalbergia sisso* showed the equilibrium adsorption of 1.33 mg/g (Bhattarai et al., 2015).

A study for the removal of As(V) and As(III) from contaminated water by Zr(IV)-loaded saponified orange waste gel showed the equilibrium adsorption capacities of 88 mg/g and 130 mg/g respectively (Muñoz et al., 1999).

A study performed for the removal of $As^{5+}$ from arsenic contaminated wastewater utilizing root of *Colocasia esculenta,* and 84.09% of $As^{5+}$ was removed from aqueous solution (Banerjee et al., 2016).

According to a study, Taro plants have a high surface area of 20.8 $m^2/g$ and a maximum adsorptive capacity of 291.56 mg/g at pH 5.5-7.0, making them an effective low-cost adsorbent for the removal of lead from aqueous solutions (Saha et al., 2017).

## 1.8 Statement of the Problems

**a. Arsenic toxicity:** Several chronic and acute diseases such as nausea, abdominal pain, diarrhea, etc. have been reported due to consumption of arsenic contaminated wastewater.

***Figure 1.2:*** *a. Different types of skin lessons; b. Keratolysis Source: Google*

**b. Difficulties with Commercially Available Adsorption Processes:** Due to the high cost and unsuitability for removing low levels of arsenic from aqueous solutions, these commercially available adsorption processes are not available and accessible to the local population.

## 1.9 Research Gap

- ❖ A cost-effective and eco-friendly optimization process is reported in limited studies.
- ❖ Comparative analysis with adsorbent materials prepared from different parts of taro plant and with other adsorbent materials has not been investigated yet.
- ❖ Regeneration and reusability of the adsorbent materials after adsorption process is a challenge, and there is not any suitable method of disposal.

## 1.10 Objective of the Study

### 1.10.1 General objective:

The general objective of the present proposed work is to prepare cost-effective activated carbon adsorbent materials from taro plant and their physico-chemical activation for the removal of arsenic ions from arsenic contaminated wastewater.

### 1.10.2 Specific objectives

- To characterize adsorbent materials prepared from different parts of the waste taro plants separately.
- To determine specific surface area of adsorbents by methylene blue method.
- To compare the maximum adsorption capacity of the adsorbent materials from different parts of taro plants.
- To study the effect of pH, contact time, initial concentration of arsenic ions on rate of adsorption.
- To study the kinetics of adsorption process and determine the nature of adsorption isotherm.
- To determine the spontaneity and feasibility of adsoption process.
- To study the adsorption mechanism of activated carbon for removal of arsenic ions from contaminated water.

# CHAPTER 2: MATERIALS AND METHODS

## 2.1 Collection of Raw Materials

Required amount of waste *Colocasia* plants were collected from agricultural lands and local markets of Kirtipur municipality of Kathmandu district shown in **Fig. 2.1**. Kirtipur municipality is located in the hilly area and is an administrative division of Kathmandu district, Nepal. Geographically, Kirtipur is located between latitudes 85$^{o}$ 13' and 85$^{o}$ 19' north and longitudes 27$^{o}$ 38' 30" and 27$^{o}$ 41' 30" east, with elevations varying from 1284 m to 1524 m above mean sea level. The Bagmati river divides the Lalitpur district from the Lalitpur sub-metropolitan city on the eastern side, while the Kathmandu metropolitan city is located on the northern side.

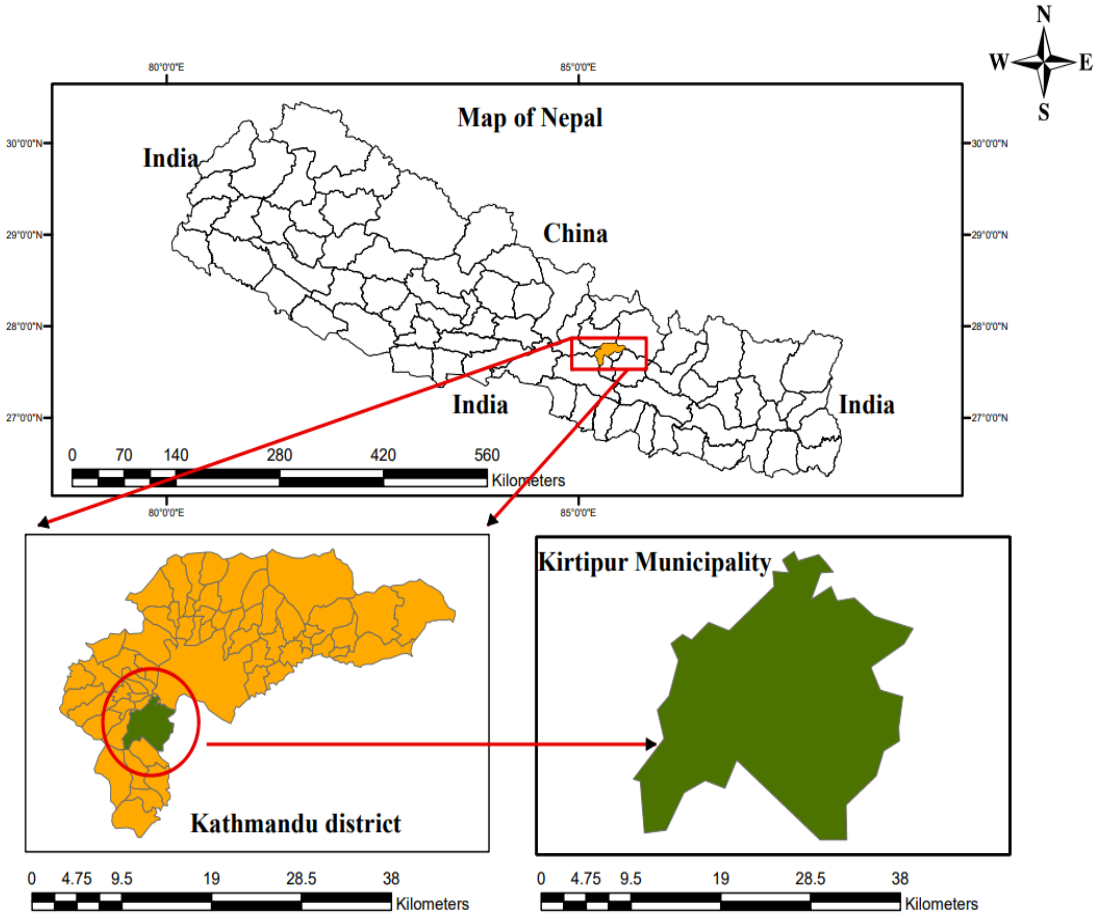


***Fig.2.1:*** *Showing districts of geographical location of study area.*

## 2.2 LR Grade Chemicals

As indicated in **Table 2.1,** all of the chemicals required for the task were acquired from various vendors. The AR/LR grade reagents were utilized without additional purification.

**Table 2.1**: Reagents and their manufacturers

| **Name of the reagents** | **Manufacturer** |
|---|---|
| Iodine, Potassium dichromate, Methylene blue, Diphenyl carbazide, Sodium azide, Sulfuric acid, Hydrochloric acid, | Merck Life Science Private Limited, Mumbai, India. |
| Arsenic trioxide | Loba-Chemie Indoaustranal Company, Mumbai, India. |
| Sodium thiosulphate, Ammonium heptamolybdate, Potassium permanganate, Sodium bicarbonate | Qualigens Fine Chemicals, Mumbai, India, |
| Potassium iodide, Nitric acid, Sodium hydroxide, Hydrazine hydrate | Thermo Fisher Scientific India Private Limited, Mumbai, India. |
| Soluble starch | Thomas Baker (Chemicals) Private Limited, Mumbai, India. |
| tablets of buffer with pH values of 4.0, 7.0, and 9.2 | Hi Media Laboratories Private Limited, Mumbai, India. |

## 2.3 Molybdenum Blue Method for the Determination of As(III)

Using this technique, the necessary volume of As(III) diluted solutions is pipette then transferred into 25 mL volumetric flasks. Each flask is filled with 4.5 mL of $H_2SO_4$ (0.5 M) and one drop of potassium permanganate (0.1 M), which are then swirled for one minute. The resultant stirred solution is then mixed with 3 mL of solutions of ammonium molybdate (0.5%) and hydrazine hydrate (0.5 M). The volume each flask is adjusted using distilled water. For the best complex formation and color development, all solutions are then allowed to sit at room temperature for 20 minutes. Using a spectrophotometer, the absorbance of each solution is measured at 840 nm in relation to the reagent blank. In an acidic solution, potassium permanganate acts as an oxidizing agent, converting As(III) to As(V). After being treated with ammonium molybdate solution, the arsenomolybdate complex is reduced with hydrazine hydrate to produce a stable, blue-colored soluble complex known as molybdenum blue, which has absorbance maxima at 840 nm. This method's detection limit is between 100 and 1000 $\mu g.L^{-1}$. The absorbance is measured by progressively diluting samples that are above the detection limit range (Lenoble, 2003).

## 2.4 Adsorption Studies

In batch tests, each stopper bottle holding a specific volume of solution with a given concentration of adsorbate is filled with a known weight of adsorbent. The mixture including the adsorbent and adsorbate is properly stirred using a thermostat mechanical shaker. Following the ideal contact period, solutions are filtered via Whattmann filter paper, and various analytical techniques are then used to assess the concentrations before and after adsorption. The primary goals of conducting batch experiments are to ascertain the pattern, mechanism, and viability of the adsorption process as well as to investigate the impact of pH and contact time on the rate of adsorption (Schiewer & Balaria, 2009).

The batch technique uses equation (2.1) to calculate the amount of adsorption (Q), as shown below.

$$Q = \frac{C_i - C_e}{m} \times V \ldots\ldots\ldots\ldots (2.1)$$

Equation (2.2) is used to determine the metal ion's adsorption effectiveness (A %), as indicated below.

$$A\% = \frac{C_i - C_e}{C_0} \times 100 \ldots\ldots\ldots\ldots (2.2)$$

Where,

$C_i$ = initial concentration of metal ion ($mg.L^{-1}$) before adsorption,

$C_e$ = equilibrium concentration of metal ion ($mg.L^{-1}$) after adsorption,

$V$ = volume of solution in liter,

$m$ = amount of biosorbent used in gram, and

$(C_i - C_e)$ = amount of metal ions adsorbed.

All adsorption experiment mean values are presented (Schiewer & Balaria, 2009).

## 2.5 Preparation of Adsorbent Materials

The sample was washed with tap water to remove the attached dust and muddy particle and worms and then with double distilled water for the eradication of contaminants. The sample was separated into its three parts: root, stalk, and leaves. A steady weight was achieved by drying the cleaned leaf sample in direct sunshine. An electric grinder was used to grind the dried sample until it had the consistency of fine powder. To achieve a consistent particle size, the powdered sample was further sieved via a 75 micron pore size sieve.

The powdered sample, known as DCLP (dried *Colocasia* leaves powder), was kept in a container with a label.

In a 100 mL R.B. flask, 30 g of dried DCLP and 100 mL of 96% concentrated sulfuric acid were combined. Following mixing, it was allowed to soak and char for 18 hours. The mixture was then refluxed for the first time using a heating mantle at a rate of 20 rpm. After six hours of constant reflux, it was exposed to sulfuric acid for two days in order to soak it further. Each time the reaction was finished, the black product that was produced was repeatedly cleaned with distilled water until it was neutral. The resulting neutral black items were dried for 24 hours at 70$^{o}$C in a convection oven. Using a mortar and pestle, the resulting final items were pulverized until each one had the consistency of fine powder. The black products obtained having acid activated carbon as predominant constituent was shortened as ACL (acid activated carbon from *Colocasia* leaves).The same process as mentioned above was repeated for roots and stalks. Both were abbreviated as ACS (acid activated carbon from *Colocasia* stalks) and ACR (acid activated carbon from *Colocasia* roots), respectively.

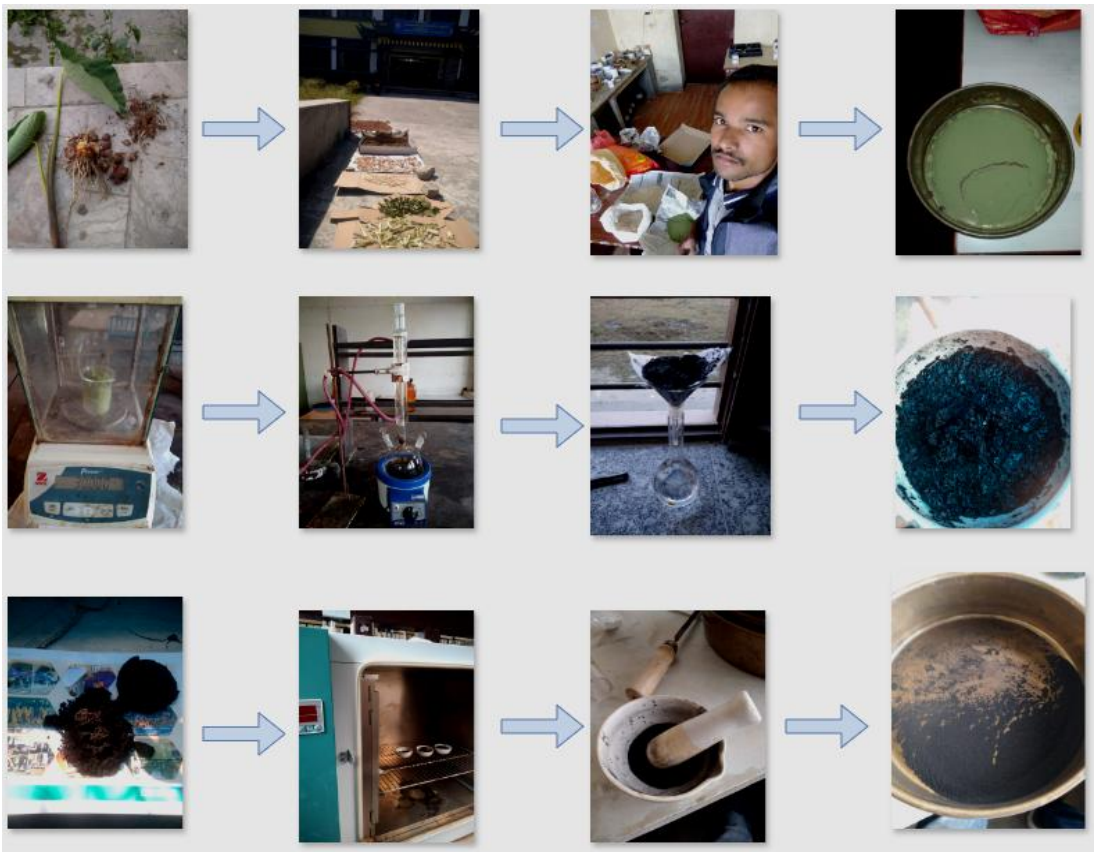

***Fig. 2.2*** *Schematic representation of adsorbent preparation using Taro (Colocasia esculenta) plants powder with Conc. $H_2SO_4$.*

## 2.6 Preparation of Stock Solutions

**Preparation of 1000 mg/L stock solution of As(III):** In a 1000 mL volumetric flask, 1.32 g of precisely weighed arsenic trioxide ($As_2O_3$, dried at 110 °C for an hour, LR Grade,) was placed in 5 mL of 10 M sodium hydroxide, agitated, and then the volume was adjusted with distilled water to the appropriate level.

149.84 g of arsenic is present in 197.84 g of $As_2O_3$

∴ 1 g of arsenic is present in 1.32 g of $As_2O_3$

1 mL of 1000 ppm arsenic = 1000 µg of arsenic

**Preparation of working solution of As(III):** Working solution of lower concentration ranging from 1 to 500 ppm was prepared by appropriate serial dilution of stock solution with distilled water.

**Making a 1000 mg.L$^{-1}$ methylene blue stock solution:** A 1000 mL volumetric flask having a small amount of distilled water was used to dissolve 1.000 g of precisely weighed and dried methylene blue. The volume was then adjusted with distilled water to reach the desired level. A 1000 mg.L$^{-1}$ stock solution was serially diluted to create the working solution of methylene blue.

**Potassium permanganate solution (0.01 M):** 0.158 g of $KMnO_4$ was dissolved in 100 mL of 1N-$H_2SO_4$ to create a potassium permanganate solution (0.01 M).

**Ammonium molybdate reagent (I):** 87.5 mL of distilled water was used to dissolve roughly 12.5 g of precisely weighed ammonium heptamolybdate [{$(NH_4)_6MO_7O_{24}.4H_2O$}, L.R. Grade]. 200 mL of purified water was carefully mixed with 140 mL of strong sulfuric acid. The sulfuric acid solution was cooled, then moved to a 500 mL volumetric flask filled with ammonium molybdate solution. Distilled water was added to bring the volume up to the required level.

**Ammonium molybdate reagent (II):** A 500 mL volumetric flask filled with 250 mL of distilled water was used to dissolve roughly 12.5 g of precisely weighed ammonium molybdate. Approximately 198 mL of ammonium molybdate reagent (I) was transferred to the 500 mL volumetric flask having ammonium molybdate reagent II in order to prepare precisely 5% of the reagent. The flask was then chilled, and the volume was adjusted with distilled water.

**Working solution of ammonium molybdate (0.5 M):** In a 100 mL volumetric flask, 10 mL of 5% ammonium molybdate reagent (II) was diluted, and the volume was adjusted with distilled water to provide a 0.5 M working solution of ammonium molybdate.

**Potassium permanganate solution (0.1 N):** An approximately 0.790 g quantity of precisely weighed LR grade $KMnO_4$ was moved into a 250 mL volumetric flask. Distilled water was added to the volume to create precisely 0.1 M solutions.
It was kept in a dark location.

**Sulfuric acid solution (3M):** In a 500 mL volumetric flask, 83.3 mL (18.1 M) $H_2SO_4$ was collected and diluted with distilled water to the appropriate level. 166.7 mL of 1.5 N $H_2SO_4$ was diluted with distilled water in a 250 mL volumetric flask to create 0.5 M $H_2SO_4$ for Cr(VI) measurement.

**Hydrazine hydrate solution (0.5 M):** A 100 mL volumetric flask containing 2.44 mL of pure hydrazine hydrate was filled with distilled water to the appropriate level.

**Sodium hydroxide solution (0.1 M):** A 500 mL volumetric flask containing around 2 g of NaOH was diluted with distilled water to the appropriate level.

**Hydrochloric acid solution (0.1 M):** A 500 mL volumetric flask was filled with approximately 4.49 mL (11.13549 M) of HCl, which was then diluted with distilled water to the appropriate level.

**Standard buffer of the pH 4.0, 7.0 and 9.2:** By mixing buffer tablets with distilled water in 100 mL volumetric flasks, buffer solutions with pH values of 4.0, 7.0, and 9.2 were created.

### 2.7 The $\lambda_{max}$ and Calibration Curves

#### 2.7.1 Determination of $\lambda_{max}$ and calibration curve for MB solution

Initially, a 250 mL volumetric flask containing 25 mL of the 1000 mg/L the initial solution was reduced to 100 mg/L using water that was distilled. After that, 50 mL of the resultant solution was taken and the volume was adjusted with distilled water to bring it down to 10 mg/L in a 500 mL volumetric flask. To create 1 to 9 ppm solutions, 2.5, 5, 7.5, 10, 12.5, 17.5, 20, and 22.5 mL solutions were made in a 25 mL volumetric flask from a 100 ppm methylene blue solution. To calculate $\lambda_{max}$, a solution with an intermediate concentration (5 mg/L) was used.

Using a spectrophotometer (2306, Electronics, India), the measurement was made between 600 and 680 nm with the blank solution adjusted to zero absorbance. At 665 nm, the highest absorption was recorded. The wavelength was fixed at 665 nm after the value of $\lambda_{max}$ was determined, and the absorbance of solutions with varying concentrations (1–10 mg/L) was measured. The calibration curve for methylene blue solution is the resultant plot of absorbance and solution concentration.

### 2.7.2 Determination of $\lambda_{max}$ and calibration curve for As(III) solution

During the calibration curve construction process, the required amounts of diluted solutions were pipetted out and poured into 25 mL volumetric flasks for the production of blank solution and arsenic solutions with concentrations of 0.1, 0.2, 0.3, 0.4, 0.5, 0.6, 0.8, and 0.9 mg $L^{-1}$. One drop of 0.1 M potassium permanganate and 4.5 mL of 0.5N sulfuric acid were added to each solution, and they were agitated for a minute. After adding 3 mL of 0.5 M hydrazine hydrate and 3 mL of 0.5% ammonium molybdate, the volume was adjusted with distilled water. To determine $\lambda_{max}$, a solution with an intermediate concentration (0.4 mg $L^{-1}$) was used. Using a spectrophotometer, the measurement was made between 810 and 870 nm with the blank solution adjusted to zero absorbance. At 840 nm, the highest absorption was recorded. The wavelength was set at 840 nm after the value of $\lambda_{max}$ was determined, and the absorbance of solutions with varying concentrations was measured. In order to determine the calibration curve, the acquired absorption data was displayed.

## 2.8 Characterization of Adsorbent Materials

### 2.8.1 XRD analysis

All the six samples like DCLP, DCSP, DCRP, ACL, ACS, and ASR were analyzed using an X-ray diffractometer with monochromatic Cu Kα radiation (D2 phaser diffractometer, Bruker, Germany) for the analysis of their phase and morphology at Nepal Academy of Science and Technology (NAST), Khumaltar, Lalitpur examined all six samples, including, for phase detection using The samples were scanned between 2θ angle of $10^{o}$ to 80°.

### 2.8.2 FTIR analysis

In order to analyze the major groups (both organic and inorganic) present in the adsorbent, dried Colocasia plants and activated *Colocasia* adsorbent materials were

examined both before and after adsorption with As(III) ions using Fourier transform infrared spectroscopy (IR Tracer 100, Shimadzu, Japan) at the Nepal Academy of Science and Technology (NAST).

### 2.8.3 Specific surface area determination techniques

Each of the three samples of activated *Colocasia* adsorbent material had its unique specific surface area measured. Methylene blue solutions with concentrations ranging from 10 to 300 mg $L^{-1}$ were placed in a regent bottle, and 25 mg of ACRs, ACSs, and ACLs powder were added separately to achieve this. After two hours of agitation in a mechanical shaker, the solutions were left for twenty-two hours. The supernatant solutions were pipetted out after half an hour. A spectrophotometer was used to measure the absorbance of the resulting supernatant solutions at 665 nm. The Langmuir adsorption isotherm was used to compute the $Q_{max}$ value, which was then used in expression (1.1), which was discussed in the previous chapter to determine the specific surface area in $m^2.g^{-1}$.

## 2.9 Adsorption Studies

### 2.9.1 Effect of pH

To investigate how pH affects arsenite adsorption, 50 mL of 137.74 mg/L arsenite solution was put into a succession of stopper bottles. Using a pH meter and 0.1 M NaOH and 0.1 M HCl, the pH of the solutions was adjusted from 2 to 10 arsenite ions, respectively. Flasks with 50 mg of ACRs, ACSs, and ACLs each were shaken for 24 hours at 220 rpm in a mechanical shaker. Each equilibrated solution was immediately filtered through Whattmann No. 41 filter paper after shaking. The starting and equilibrium concentrations of arsenite ions were ascertained using the molybdenum blue technique, respectively. The computed values of the initial and equilibrium concentrations were used to calculate the adsorption efficiency in each instance.

### 2.9.2 Adsorption isotherm studies

Under ideal pH conditions, the impact of arsenite concentrations on adsorption was investigated. 50 mL of arsenite solutions with starting concentrations varying from 7.91 to 228.62 mg/L were mixed with 50 mg of ACS. Until the equilibration time was reached, the solution was shaken at 220 rpm. The solution was immediately filtered through Whattmann No. 41 filter paper after shaking. Arsenite's initial and

equilibrium concentrations were ascertained using the molybdenum blue method. The adsorption isotherm was studied using the two most popular models, Freundlich and Langmuir.

### 2.9.3 Kinetics studies

It was investigated how kinetics affected the adsorption of arsenite removal. Here, 50 mL of arsenite solutions with starting concentrations ranging from 169.069 to 200. 39 mg/L were mixed with 50 mg of ACS. Arsenite ions were shaken for varying periods of time, from five minutes to twenty-four hours, at 220 rpm in a mechanical shaker. Each solution was immediately filtered through Whattmann No. 41 filter paper after being shaken. The initial and equilibrium arsenite ions concentrations were determined using the molybdenum blue method. Pseudo-first and pseudo-second order kinetic models were used to test the acquired data.

# CHAPTER 3: RESULTS AND DISCUSSIONS

## 3.1 Characterization of Adsorbent Materials

### 3.1.1 X-Ray Diffraction (XRD) analysis

The XRD patterns of all three types of raw materials (DCRP, DCSP, and DCLP) and their respective activated carbons (Such as ACR, ACS, and ACL) were obtained. All the XRD patterns of raw and their activated carbons are shown in following **Fig. 3.1**. The XRD graph has been plotted between angle of diffraction (2θ, degree) as abscissa and intensity (a.u.) as ordinate. X-axis represents the diffraction angle, used to identify crystalline phases and y-axis represents the intensity of diffracted x-rays, indicating the degree of crystallinity.

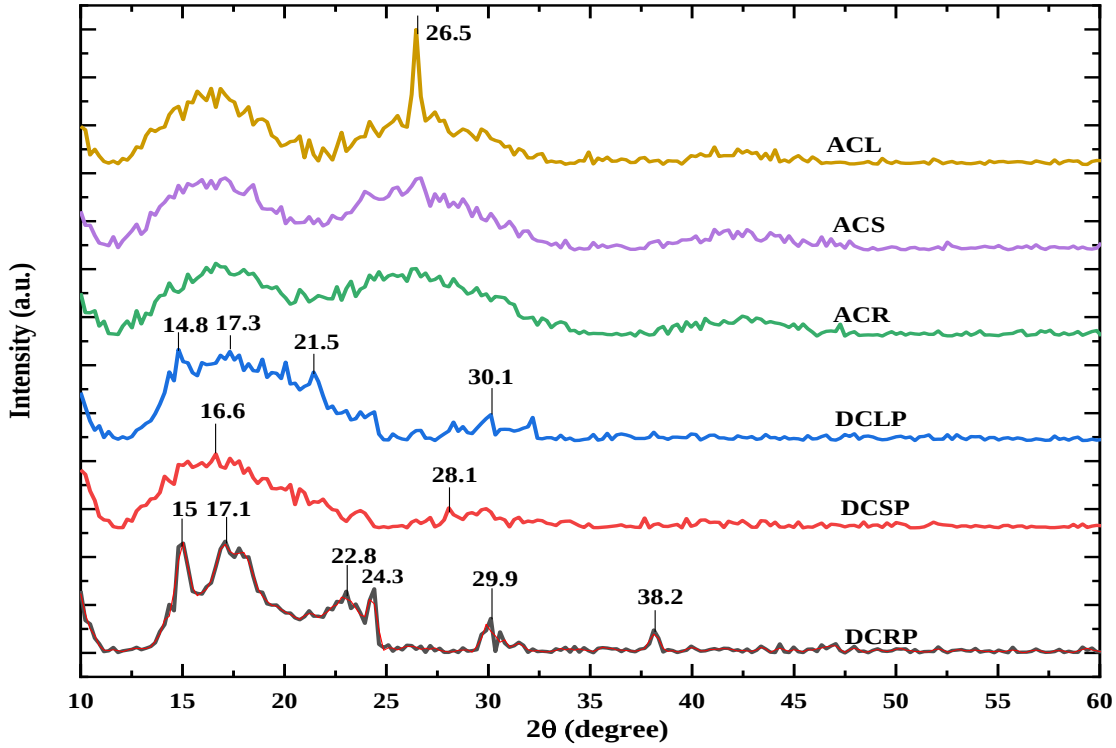


***Fig. 3.1**: XRD patterns of dried Colocasia root powder (DCRP), dried Colocasia stalk powder (DCSP), dried Colocasia leaves leave powder (DCLP), activated Colocasia root (ACR), activated Colocasia stalk (ACS), and activated leaves (ACL).*

DCRP, DCSP, and DCLP show sharp peaks at 16.6°, 29.9° and 40.6°. These peaks indicate more crystalline regions which are typical in natural plant-based materials. The distinct peaks suggest the presence of some crystalline phases likely due to silica or cellulose.

Whereas ACR, ACS, and ACL show weak and broad diffraction peaks at specific 2θ values. Broad peaks are characteristics of amorphous structure. ACL displayed a sharp peak at 26.5°, often attributed to graphitic carbon (002 plane) or silica.

Raw taro materials DCRP, DCSP, and DCLP show crystalline nature but after activation the samples ACR, ACS, and ACL became amorphous, confirming successful transformation into adsorbent materials.

### 3.1.2 FTIR analysis

FTIR analysis is used for identifying functional groups on adsorbent materials and potential molecular bonds between their chemical constituents. It is plotted as wavenumber ($cm^{-1}$) versus transmittance (%). The FTIR spectra of all three types of raw materials and their respective activated carbons were taken and are shown in following **Fig. 3.2**:

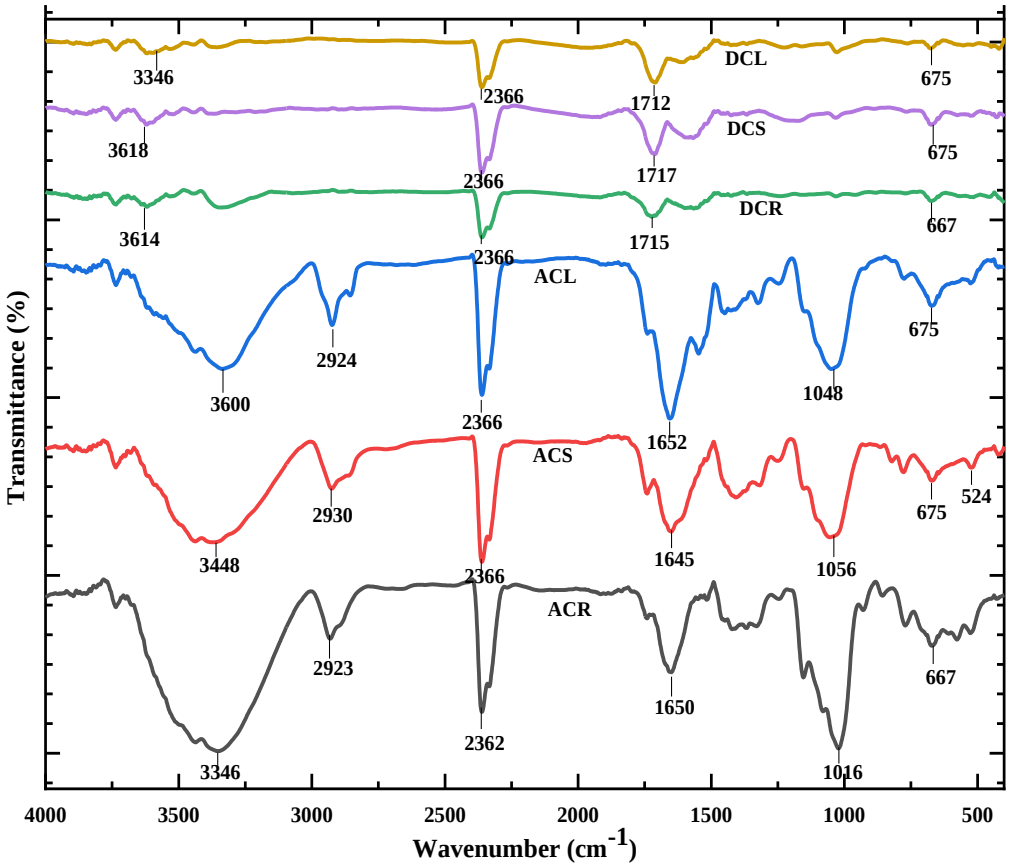


***Fig. 3.2:*** *FTIR patterns dried Colocasia root powder (DCRP), dried Colocasia stalk powder (DCSP), dried Colocasia leaves (DCLP), activated Colocasia root (ACRP), activated Colocasia stalk powder (ACSP), and activated Colocasia leaves (ACLP).*

The spectrum of DCRP and ACR has a broad band between 3500-3650 $cm^{-1}$ showing hydrogen bonded monomeric carboxylic acid (C = O), the values of aliphatic C-H stretching were 2923, 1402, and 2848 $cm^{-1}$. The C=C of arene was measured between 1600 and 1670 $cm^{-1}$.Strong and sharp peaks in between 1690-1760 had been observed showing C=O of aldehyde, ketone, carboxylic esters.

The spectrum of DCSP and ACS has a broad band between 3500-3650 $cm^{-1}$ showing hydrogen bonded monomeric carboxylic acid (C = O), We observed aliphatic C-H stretching at 2923, 1402, and 2848 $cm^{-1}$. The C=C of arene was measured between 1600 and 1670 $cm^{-1}$. Strong and sharp peaks in between 1690-1760 $cm^{-1}$ had been observed showing C=O of aldehyde, ketone, carboxylic esters.

The spectrum of DCL and ACL has a broad band between 3500-3650 $cm^{-1}$ showing hydrogen bonded monomeric carboxylic acid (C = O), The values of aliphatic C-H stretching were 2923, 1402, and 2848 cm-1. The C=C of arene was measured between 1600 and 1670 $cm^{-1}$. Strong and sharp peaks in between 1690-1760 $cm^{-1}$ had been observed showing C=O of aldehyde, ketone, carboxylic esters.

All activated samples (ACL, ACS, ACR) showed key functional groups such as –OH, C–H, C=O, and C–O. ACS exhibits the richest and deepest peaks, suggesting it may have the highest adsorption potential due to higher functional group diversity.

### 3.2 Determination of Specific Surface Area of Activated Adsorbent Materials

#### 3.2.1 Determination of $\lambda_{max}$ for MB Solution

**Figure 3.3** displays the absorbance of MB solution versus wavelength curve. The wavelength for maximum absorbance was measured at 665 nm, which is in agreement with previous report (Thapa & Pokhrel, 2013).

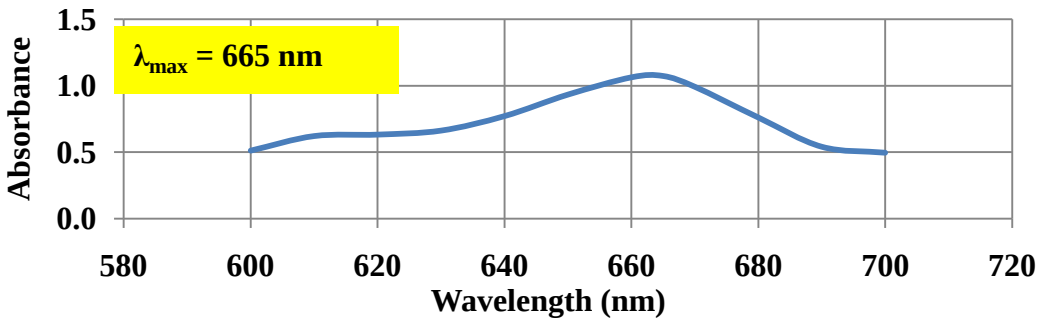


***Fig. 3.3:*** *A plot of Absorbance versus wavelength at concentration of 5 mg/L MB solution.*

### 3.2.2 Calibration Curve of the MB Solution

The calibration curve for methylene blue solution is shown in **Fig. 3.4**. It was found to follow Beer-Lambert's rule and be linear up to 10 ppm. More dilution was needed to determine the absorbance of the extremely concentrated methylene blue solution.

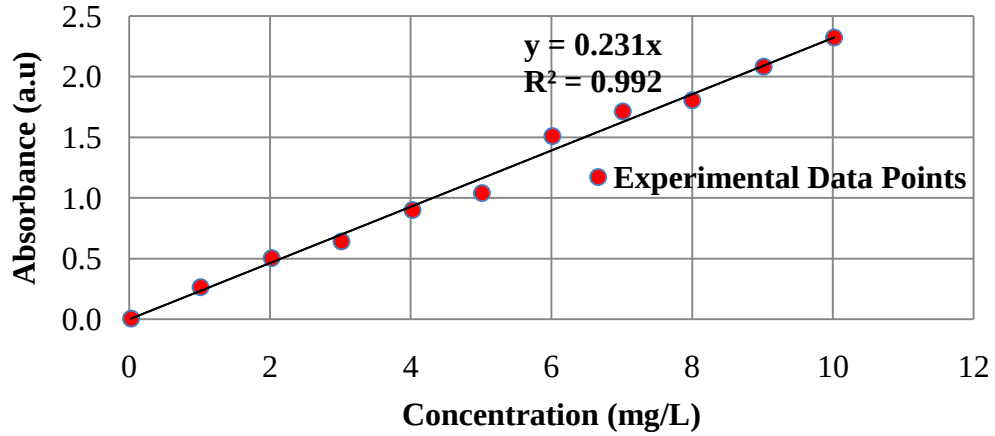


***Fig. 3.4:*** *A plot of absorbance as a function of the concentration of MB solution.*

### 3.2.3 Specific Surface Area Measurement

In order for the determination of specific surface area of the adsorbent materials, linearized plots of equilibrium concentration of methylene blue versus $\frac{C_e}{Q_e}$ for all three adsorbent materials were obtained. **Figure 3.5** displays the linearized Langmuir curves for ACS, ACL, and ACR respectively.

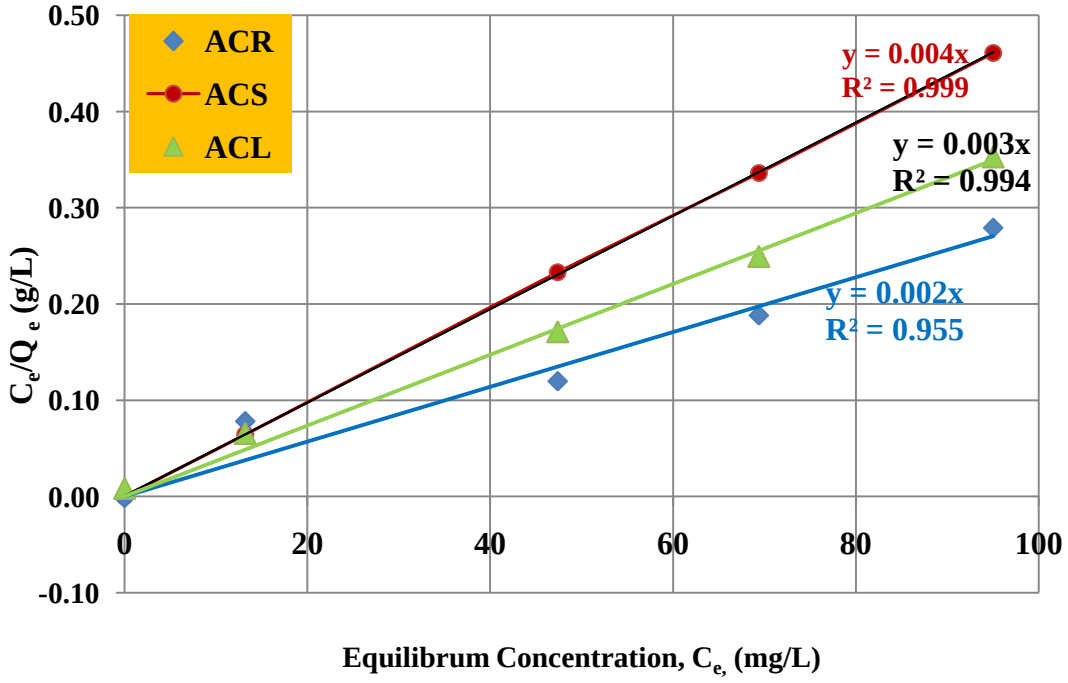


***Fig. 3.5:*** *A plot of $C_e/Q_e$ versus $C_e$ of ACR, ACS, and ACL*

With the help of the slope of each and every linearized plot the maximum methylene blue adsorption capacity ($Q_{max}$) of each adsorbent material was calculated with the help of equation (1.3). After calculating the values of $Q_{max,}$ the specific surface areas of all the three adsorbent materials were calculated using **equation (1.1)**.

The specific surface areas of all three adsorbent materials are shown in **Fig. 3.6**.

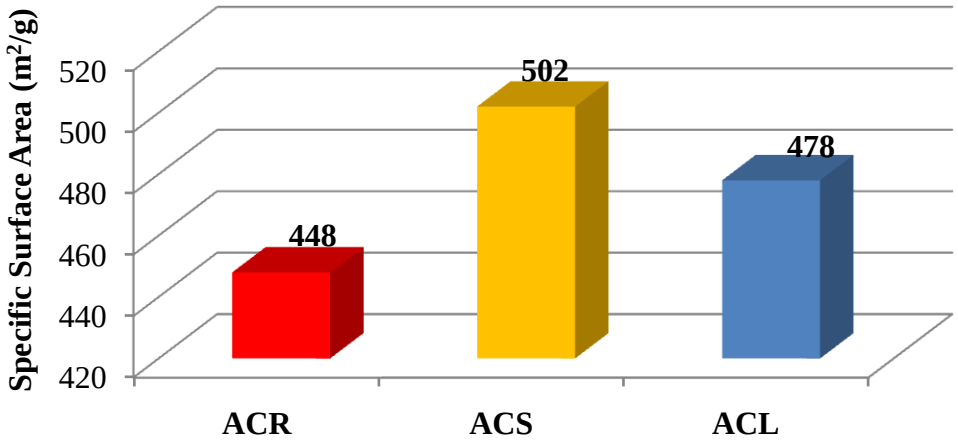


***Fig. 3.6:*** *Comparative study of SSA on different adsorbents.*

The bar diagrams in **Figure 3.6** displays the specific surface area of the three adsorbent materials. The specific surface areas were found to be 448, 502 and 478 $m^2g^{-1}$ for ACR, ACS, and ACL, respectively. Different chemical compositions and internal structure might be the cause of different specific surface area of ACR and ACL when compared to ACS.

### 3.3 Determination of $\lambda_{max}$ of As(III) Solution

**Figure 3.7** displays the absorbance versus wavelength plot for As(III) solutions. For As(III), the highest absorbance was measured at 840 nm, which is in good agreement with the values found in the literature (Thapa & Pokhrel, 2013).

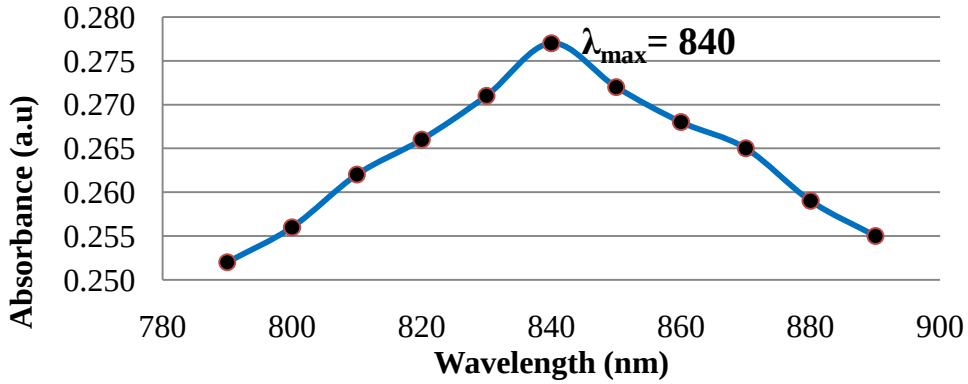


***Fig. 3.7:*** *Plots of absorbance as the function of wavelength of As(III) solutions*

### 3.4 Calibration Curves of As(III) Ion Solution

**Figure 3.8** displays the calibration curves related to As(III). In all cases, the curves were found to be linear up to the concentration ranges for As(III) between 1 and 6 mg/L. For the specified concentration range, Beer-Lambert's law was thus followed in every instance.

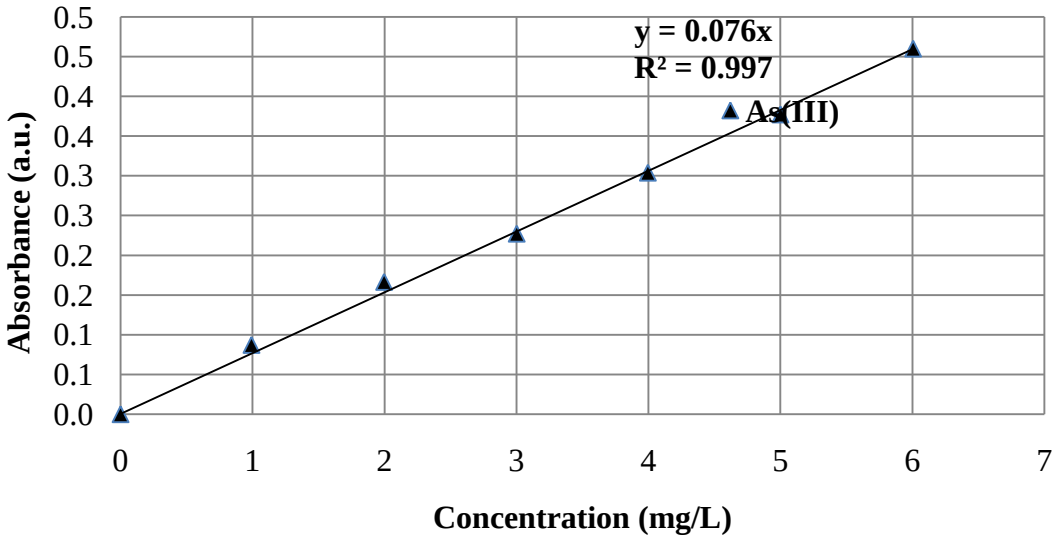


***Fig. 3.8:*** *A plot of absorbance as the function of concentration of As(III) ion solutions.*

### 3.5 Effect of pH

The data obtained from XRD, FTIR spectra, and the specific surface area determination for ACS suggest that it may have the highest adsorption potential due to a greater diversity of functional groups and highest specific surface area (502 $m^2/g$). Therefore, ACS was considered the most effective among the three activated carbons and was subsequently used for batch experiments and As(III) adsorption studies.

As illustrated below, **Fig. 3.9** depicts the outcomes of the adsorptive removal of As (III) ions as a function of pH:

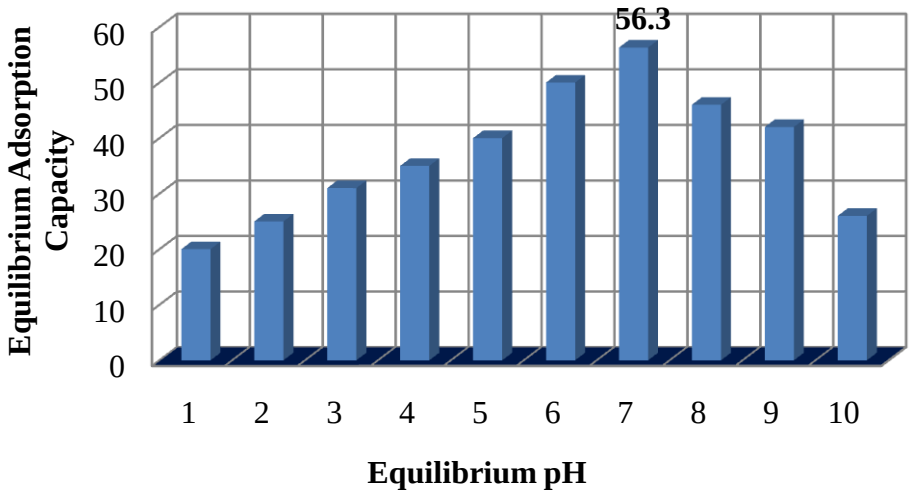


***Fig. 3.9:*** *Effect of pH for the adsorption of As(III) onto ACS.*

**Effect of pH on Arsenic adsorption**

In the aqueous phase, arsenate species are found as $H_3AsO_4$ at pH less than 2.2, $H_2AsO_4^-$ at pH between 2.2 and 6.98, $HAsO_4^{2-}$ at pH 6.98–11.5, and $AsO_4^{3-}$ at pH greater than 11.5 (Chang et al., 2010). On the other hand, arsenite species exist as $AsO_2^-$ at pH values more than 9 and as neutral $H_3AsO_3$ at pH values between 1 and 9 (Zhu et al., 2015). Continuously raising the pH of the solution containing the As(III) ion altered the sorbent's adsorption yield. It was found that the adsorption capacity and adsorption percentage were lowest at pH 1 and highest at pH 7. $H^+$ ion mobility and concentration are generally high at low pH. At pH 7 (neutral condition), As(III) exists mainly as $H_3AsO_3$, which is uncharged. this neutral nature means it does not strongly repel or attract charged surfaces. The surface might have slightly positive or neutral surface charge around pH 7, which allows van der Waals forces, hydrogen bonding, or ligand exchange to occur. The adsorption at pH 7 was maximum that might be because at lower pH ($< 5$), excess $H^+$ ions competed with As(III) for active sites. At higher pH ($> 8$), the surface might become more negative, and the adsorption of neutral As(III) became less favorable due to reduced attraction.

The ideal pH for arsenite adsorption, as determined by experiment, was 7. According to FTIR data, the presence of a weakly acidic hydroxyl group may have contributed to the partial ion exchange process, which is why the experimentally measured value fluctuated from the value found in the literature. At pH values higher than 7, As(III) is present in an anionic state and does not adsorb well on negatively charged surfaces..

Because of the presence of certain arsenite species that are not oxidized, physisorption also appears to play a crucial role during the adsorption process in this study project. For As(III), the ideal pH value for the remaining batch tests was set at 7.

### 3.6 Batch Adsorption Isotherm Studies

The adsorption capacity of ACS was estimated by As(III) adsorption isotherm tests, which used adsorbent dosages of 50 mg, agitation speeds of 220 rpm, and concentration variations in the range 7.91-228.62 mg.$L^{-1}$ for As(III). The linearized Langmuir and Freundlich plots were obtained as shown in **Fig. 3.10** and **Fig. 3.11.** The Langmuir and Freundlich parameters were computed using the slopes and intercepts of the linearized Langmuir and Freundlich plots and tabulated in **Table 3.1**. The maximum adsorption capacity for As(III) by ACS was obtained from the slope of linearized Langmuir curve was 62.5 mg/g.

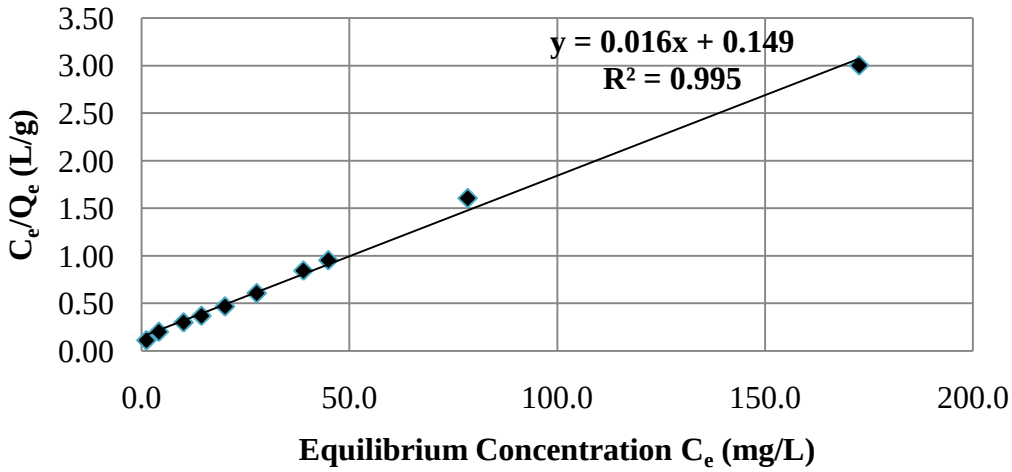


***Fig. 3.10:*** *The linearized Langmuir curve for the adsorption of As (III) concentrate onto ACS.*

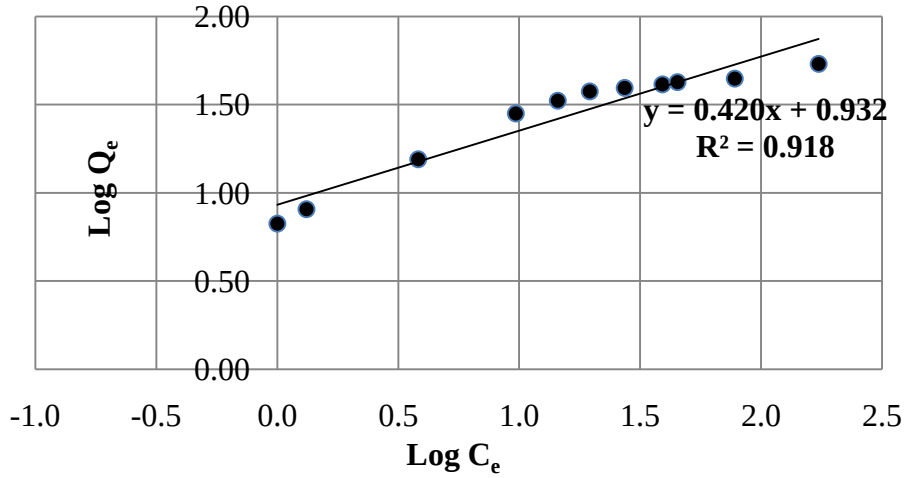


***Fig. 3.11:*** *The linearized Freundlich curve for the adsorption of As (III) onto ACS.*

**Table 3.1:** Parameters of Langmuir and Freundlich constants

| **Ions** | **Langmuir model** | | | | | |
|---|---|---|---|---|---|---|
| **As(III) ions** | $Q_{max.}$ (mg/g) | b (L/mg) | $R^2$ | ΔG (kJ/mol) | $\chi^2$ | $K_L$ |
| | 62.5 | 0.186 | 0.984 | -22 | 4.12 | 0.843 |
| | **Freundlich Model** | | | | | |
| | $K_F$ [(mg/g)(L/mg)$^{1/2}$] | | n | $R^2$ | $\chi^2$ | |
| | 18.74 | | 4.3 | 0.882 | 26.16 | |

**Figure 3.12** displays the As(III) ion adsorption versus equilibrium concentration plot for As (III). In each instance, the computed Langmuir curve fits the experimental data quite well. The Langmuir isotherm fits the data more accurately than the Freundlich isotherm in every instance; consequently, monolayer adsorption occurred on the surface of ACS, with very good coefficient of determination of 0.995. Maximum absorption capacity ($Q_{max}$) measured from non-linear Langmuir curve was 62.5 mg/g$^{-1}$. The smaller value of $\chi^2$ for the Langmuir model in comparison to the Freundlich model demonstrated that the Langmuir adsorption isotherm was the best-fitting model. The calculated value of free energy ΔG was –22 kJ/mol$^{-1}$ for adsorption. The spontaneous physico-chemical adsorption of As(III) on ACS was confirmed by the negative free energy (ΔG) measurements. The value of $K_L$ was found to be 0.843 which was in between 0 and 1 indicating favorable adsorption.

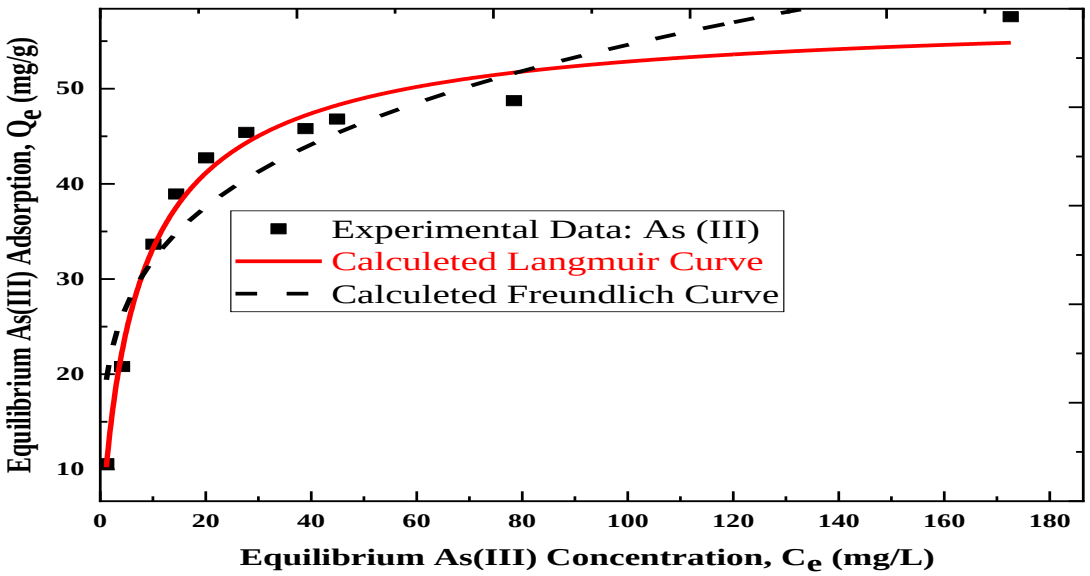


***Fig. 3.12:*** *Comparative study of Langmuir and Freundlich adsorption isotherms of Arsenic ions onto ACS.*

### 3.7 Batch Kinetic Studies

Pseudo-first order and pseudo-second order kinetic models were used to analyze the experiment in order to determine the best-fitting kinetic model and assess the adsorption mechanism. The pseudo-first order model plotted $log(Q_e - Q_t)$ against t whereas the pseudo-second order model plotted $\frac{t}{Q_t}$ against t. The equilibration time and metal ion binding rate on the chemically altered adsorbent surface are ascertained by kinetic tests. **Figure 3.13** and **Fig. 3.14** display the graphs that explain pseudo-first and pseudo-second order kinetic data. The plots of pseudo-first order and pseudo-second order models produced the straight lines. The coefficient of determination ($R^2$) for pseudo-first order and pseudo second order kinetics were 0.865 and 0.999, respectively for As(III). But compared to pseudo-first order kinetics, pseudo-second order kinetics has a greater $Q_e$ and $R^2$ values indicating pseudo-second order kinetics was the best fitting model for As(III) adsorption onto ACS.

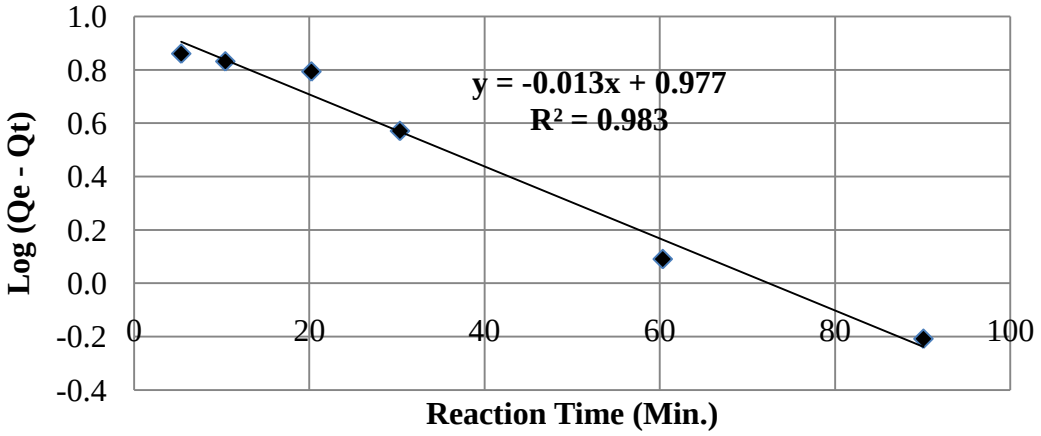


***Fig. 3.13:*** *As (III) ion adsorption onto ACS using a pseudo-first order kinetic mod*

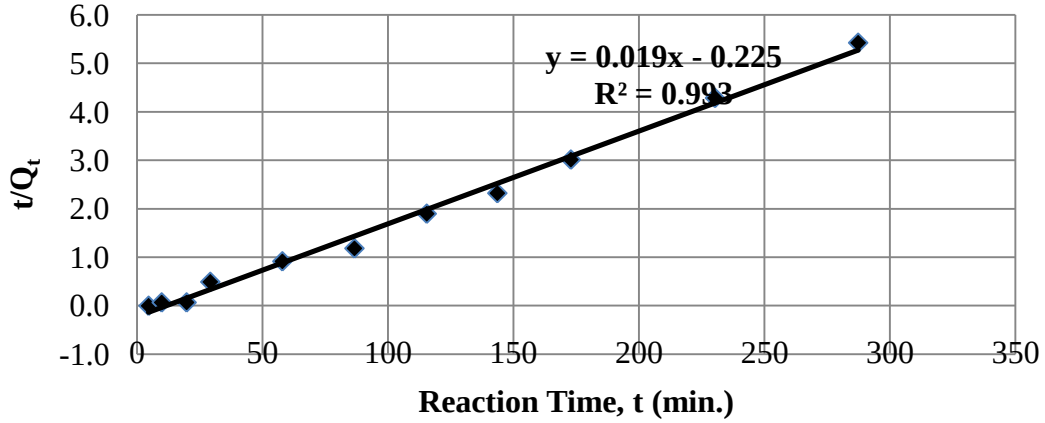


***Fig. 3.14:*** *As (III) ion adsorption onto ACS using pseudo-first order kinetic model.*

The kinetic parameters obtained from the slope and intercepts of **Figures 3.21** and **3.22** are shown in **Table 3.2**.

**Table 3.2:** Kinetic order and rate constants for As (III) adsorption onto ACS

| **order** | | **Slope** | **Intercept** | **$K_1$** | **$K_2$** | **$Q_e$** | **$R^2$** |
|---|---|---|---|---|---|---|---|
| 1st | Arsenic | 0.011 | 1.160 | 0.025 | | 3.191 | 0.865 |
| 2nd | Arsenic | 0.019 | 0.019 | | 0.018 | 53.8 | 0.999 |

The rate constants for the adsorption of As(III) onto ACS fall was 0.01830 g/mg·min, also indicating pseudo-second order kinetics.

**Figure 3.15** displays a kinetic curve that plots the equilibrium adsorption capacity against time. In the first stage for As(III), the amount of adsorption increases dramatically as the contact time increases. It then increased steadily to attain the equilibrium level in less than 50 minutes. Increasing the contact duration further had no discernible impact on the amount of adsorption. In conclusion, the remaining batch studies have a predetermined shaking time of 50 minutes each. The availability of additional active sites in the early stages is what causes the initial significant increase in adsorption capacity. Adsorption causes the number of active sites to decrease with time, reaching an equilibrium value after a predetermined amount of time. In order to achieve equilibrium after a specific amount of time, the equilibrium adsorption capacity was progressively raised.

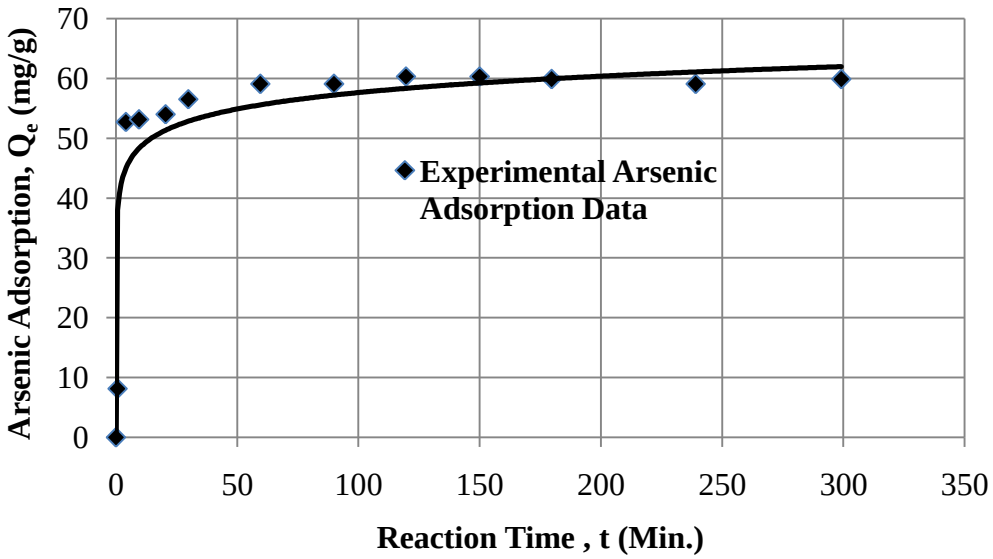


***Fig. 3.15:*** *Kinetic plots for the adsorption of arsenite on ACS.*

### 3.8 Mechanism of As (III) Adsorption

The complicated pattern of adsorption mechanism incorporating many mechanisms is indicated by the highest adsorption at pH 7 and the free energies of adsorption (ΔG) in the range of -22 kJ/mol$^{-1}$ for As (III). Both physisorption and chemisorptions follow the adsorption process. Chemisorption is caused by loosely bound hydroxyl groups that are available for the ion exchange process, whereas physisorption is caused by the pores found in activated carbon. The intraparticle diffusion model is frequently employed to ascertain the adsorption mechanism. **Figure 3.16** shows a plot between adsorption capacity, $Q_{t,}$ (mg/g) against the square root of time ($\sqrt{t}$).

Since the line obtained did not pass through the origin, the rate limiting step was not governed by the intraparticle diffusion model. The $K_{id}$ and $R^2$ values obtained from the plot are 0.5058 and 0.7081 respectively.

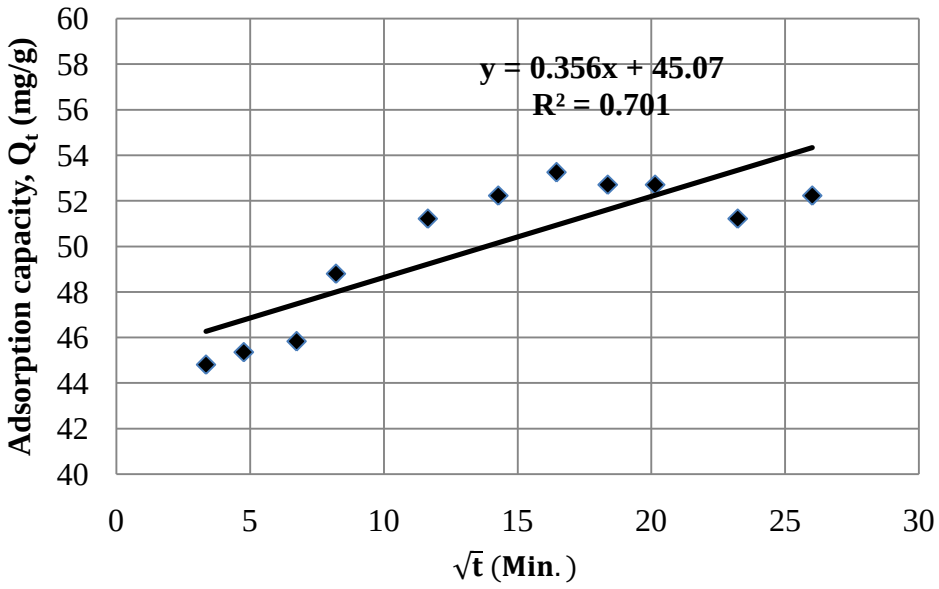


***Fig. 3.16:*** *Plot of $Q_t$ versus $\sqrt{t}$ for the adsorption of As(III) on ACS.*

**Figure 3.17** below displays the FTIR spectra before and after As(III) adsorption of activated carbon from ACS.

Even in the range of 3280-3460 cm$^{-1}$, no broad band of hydroxyl peak was found in the spectra that were produced following the adsorption of arsenite ions. The involvement of hydroxyl group in the adsorption process may be the cause of diminishing hydroxyl peaks. Following arsenic ion adsorption, the background $CO_2$ peaks observed at 2200–2400 cm$^{-1}$ were largely reduced, indicating that arsenic ions are preferentially adsorbed on the adsorbent.

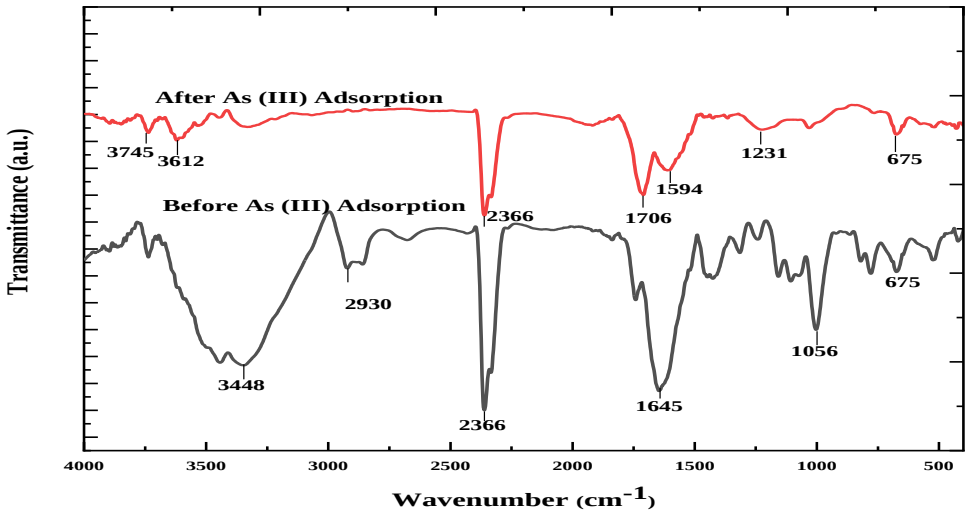


***Fig. 3.17:*** *FTIR Spectra of before and after As (III) adsorption of ACS.*

### 3.9 Comparison of the Maximum Adsorption Capacity ($Q_{max}$)

The most recent literature review of the different adsorbents with varying adsorption capacities are listed in **Table 3.3**.

**Table 3.3**: Comparison of the Maximum Adsorption Capacity ($Q_{max.}$) for As (III)

| **S. No.** | **Adsorbent** | **$Q_{max}$** (mg/g) | **Source** |
|---|---|---|---|
| 1. | Quaternized rice husk | 18.98 | (Kanel et al., 2023) |
| 2. | Fe/Cu nanoparticles | 19.68 | (Babaee et al., 2018) |
| 3. | Fe (III) loaded pomegranate waste | 50 | (Thapa & Pokhrel, 2013) |
| 4. | Activated carbon from rubber tires that has been altered with an alumina composite | 14.28 | (Karmacharya et al., 2016) |
| 5. | Composite of rubber-alumina tyre | 13.51 | (Karmacharya et al., 2016) |
| 6. | Fe-Mn modified granular activated carbon | 2.87 | (Nikić et al., 2019) |
| 7. | Staphylococcus Fe-treated biomass | 54.35 | (Aryal et al., 2010) |
| 8. | Iron oxide impregnated activated alumina | 0.858 | (Kuriakose et al., 2004) |
| 9. | Fe (III) loaded phosphorylated *Dalbergia sissoo* saw dust | 1.33 | (Bhattarai et al., 2015) |
| 10. | saponified orange waste gel loaded with Zr (IV) | 130 | (Hu et al., 2012) |
| 11. | Fe(III) loaded phosphorylated orange waste gel | 0.91 | (Ghimire, 2013) |
| 12. | orange waste gels loaded with Lanthanum (III) and Cerium (III) | 43 | (Biswas, Inoue, Inoue, et al., 2008) |
| 13. | Activated spinach leaves (ASL-2) | 58.480 | (Jha & Jha., 2021) |
| **14.** | **Activated Colocasia Stalk (ACS)** | **62.5** | **Present work** |

The As(III) loaded $Q_{max}$ values of adsorbent were significantly greater than those of the majority of other adsorbents that have been reported.

### 3.10 Desorption Studies

Desorption was carried out using a 0.01 M to 2 M NaOH solution. The ideal pH, according to the pH impact study, was 9. It suggests that at pH >9, the biosorption of arsenite anion is less favorable.

The desorption percentage of adsorbed arsenite anion versus NaOH concentration is shown in **Fig. 3.18**. The desorption percentage of As(III) rises as the NaOH concentration is increased from 0.01M to 2M. Thus, using 2M NaOH, 92.21% efficient desorption was achieved. This implies that ACS is a useful adsorbent for the upcoming cycle because to its regeneration capability.

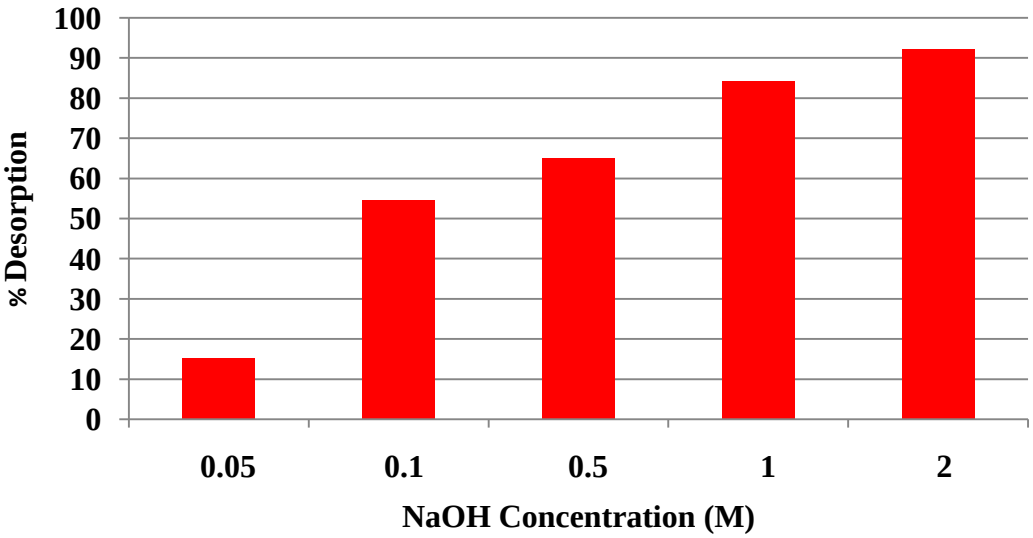


***Fig. 3.18:*** *Desorption % of As (III) versus molar concentration of NaOH.*

# CHAPTER 4: CONCLUSIONS AND SUGGESTIONS

## 4.1 Conclusions

In this study, three distinct low-cost adsorbent materials namely ACR, ACS, and ACL were made from the root, stalk, and leaves of waste Taro *(Colocasia esculenta)*. The adsorbent materials were characterized using the FTIR, XRD, and MBAM. Weak and broad diffraction peaks were found in the adsorbent's crystal plane at 2θ angles. A distinct and sharp peak was obtained at $26.5^{o}$ showed residual silica or graphite for ACL. Thus, the development of amorphous activated carbon was strongly supported by XRD examination. These groups are in charge of As(III) adsorption, according to the hydroxyl peaks that were acquired for FTIR analysis. Using the MBAM, the specific surface area values for ACR, ACS, and ACL were 448, 502, and, 478 $m^2/g$ respectively. With a high SSA of 502 $m^2/g$, ACS was shown to be the best adsorbent among the three. Thus, ACS was selected for additional research.

- As(III) adsorption was a pH-dependent mechanism that peaked at pH 7.
- As(III) adsorption on ACS has an equilibrium period of less than 50 minutes.
- The pseudo-second order kinetics model and the Langmuir model both fit perfectly with the experimental results.
- The equilibrium adsorption capacities for As(III) determined from linearized Langmuir model was 62.5 mg/g.
- The Langmuir equation for As (III) yielded negative ΔG values in the range of −22 kJ/mol, indicating that the adsorption process was physico-chemical, feasible, and spontaneous.
- Using 2 M NaOH, 92.21% efficient desorption was achieved in three cycles

## 4.2 Suggestions for Further Work

Advanced instrumental tools like optical microscopy (OP), scanning, and transmission electron microscopes (SEM and TEM) can be used to further characterize adsorbent materials. With the autosorb device, the most precise specific surface area, pore volume, pore diameter, and microporous and mesoporous nature may be determined. If the right advanced laboratory conditions and equipment are available, the adsorption of As(III) on ACS can be improved. The ability of activated carbon to adsorb As(III) from aqueous solution may be enhanced by further chemical treatments such as metal loading, phosphorylation followed by $H_2SO_4$ activation, etc. Real wastewater samples can be used to study As (III) adsorption utilizing ACS.

## REFERENCES


Aggett, J., & Aspell, A.C. The determination of As(III) and total arsenic by atomic-absorption spectroscopy. *The Analyst*, **1976**, *101*(1202), 341. https://doi.org/10.1039/an9760100341

Agrafioti, E., Kalderis, D., & Diamadopoulos, E. Arsenic and chromium removal from water using biochars derived from rice husk, organic solid wastes and sewage sludge. *Journal of Environmental Management*, **2014**, *133*, 309–314. https://doi.org/10.1016/j.jenvman.2013.12.007

Ahluwalia, S. S., & Goyal, D. Microbial and plant derived biomass for removal of heavy metals from wastewater. *Bioresource Technology*, **2007**, *98*(12), 2243–2257. https://doi.org/10.1016/j.biortech.2005.12.006

Ahmed, M. J., & Theydan, S. K. Physical and chemical characteristics of activated carbon prepared by pyrolysis of chemically treated date stones and its ability to adsorb organics. *Powder Technology*, **2012**, *229*, 237–245. https://doi.org/10.1016/j.powtec.2012.06.043

Anzai, A., Chowdhury, S. A., & DeAngelis, G. C. Coding of Stereoscopic Depth Information in Visual Areas V3 and V3A. *Journal of Neuroscience*, **2011**, *31*(28), 10270–10282. https://doi.org/10.1523/JNEUROSCI.5956-10.2011

Aryal, M., Ziagova, M., & Liakopoulou-Kyriakides, M. Study on arsenic biosorption using Fe(III)-treated biomass of Staphylococcus xylosus. *Chemical Engineering Journal*, **2010**, *162*(1), 178–185. https://doi.org/10.1016/j.cej.2010.05.026

Babaee, Y., Mulligan, C. N., & Rahaman, M. S. Removal of As( III ) and As(V) from aqueous solutions through adsorption by Fe/Cu nanoparticles. *Journal of Chemical Technology & Biotechnology*, **2018**, *93*(1), 63–71. https://doi.org/10.1002/jctb.5320

Baby, J., Raj, J., Biby, E., Sankarganesh, P., Jeevitha, M., Ajisha, S., & Rajan, S. Toxic effect of heavy metals on aquatic environment. *International Journal of Biological and Chemical Sciences*, **2011**, *4*(4). https://doi.org/10.4314/ijbcs.v4i4.62976

Banerjee, S., Mukherjee, S., LaminKa-ot, A., Joshi, S. R., Mandal, T., & Halder, G. Biosorptive uptake of $Fe^{2+}$ , $Cu^{2+}$ and $As^{5+}$ by activated biochar derived from Colocasia esculenta: Isotherm, kinetics, thermodynamics, and cost estimation. *Journal of Advanced Research*, **2016**, *7*(5), 597–610.

https://doi.org/10.1016/j.jare.2016.06.002

Bhattarai, P., Bohra, K. P., & Pokhrel, M. R. Adsorptive Removal of As(III) from Aqueous Solution. *Journal of Institute of Science and Technology*, **2015**, *19*(1), 150–154. https://doi.org/10.3126/jist.v19i1.13841

Biswas, B. K., Inoue, J., Inoue, K., Ghimire, K. N., Harada, H., Ohto, K., & Kawakita, H. Adsorptive removal of As(V) and As(III) from water by a Zr(IV)-loaded orange waste gel. *Journal of Hazardous Materials*, **2008**, *154*(1–3), 1066–1074. https://doi.org/10.1016/j.jhazmat.2007.11.030

Biswas, B. K., Inoue, K., Ghimire, K. N., Kawakita, H., Ohto, K., & Harada, H. Effective Removal of Arsenic with Lanthanum(III)- and Cerium(III)-loaded Orange Waste Gels. *Separation Science and Technology*, **2008**, *43*(8), 2144–2165. https://doi.org/10.1080/01496390802064075

Boampong, R., Aboagye, L. M., Nyadanu, D., Essilfie, M. E., & Adu Amoah, R. Biochemical Charcterization of Some Taro ( *Colocasia esculenta* L. Schott) Germplasm in Ghana. *Advances in Agriculture*, **2019**, 1–7. https://doi.org/10.1155/2019/1965761

Campos, N. F., Barbosa, C. M., Rodríguez-Díaz, J. M., & Duarte, M. M. Removal of naphthenic acids using activated charcoal: Kinetic and equilibrium studies. *Adsorption Science & Technology*, **2018**, *36*(7–8), 1405–1421. https://doi.org/10.1177/0263617418773844

Chang, Q., Lin, W., & Ying, W. Preparation of iron-impregnated granular activated carbon for arsenic removal from drinking water. *Journal of Hazardous Materials*, **2010**, *184*(1–3), 515–522. https://doi.org/10.1016/j.jhazmat.2010.08.066

Feng, N., Guo, X., Liang, S., Zhu, Y., & Liu, J. Biosorption of heavy metals from aqueous solutions by chemically modified orange peel. *Journal of Hazardous Materials*, **2011**, *185*(1), 49–54. https://doi.org/10.1016/j.jhazmat.2010.08.114

Ferreira, M. A., & Barros, A. A. Determination of As(III) and arsenic(V) in natural waters by cathodic stripping voltammetry at a hanging mercury drop electrode. *Analytica Chimica Acta.*, **2002**, *459*(1), 151–159. https://doi.org/10.1016/S0003-2670(02)00086-7

Freundlich, Herbert., & Heller, Wilfried. The Adsorption of *cis*—And *trans* - Azobenzene. *Journal of the American Chemical Society*, **1939**, *61*(8), 2228–2230.

https://doi.org/10.1021/ja01877a071

Gallardo, M. V., Bohari, Y., Astruc, A., Potin-Gautier, M., & Astruc, M. Speciation analysis of arsenic in environmental solids Reference Materials by high-performance liquid chromatography–hydride generation–atomic fluorescence spectrometry following orthophosphoric acid extraction. *Analytica Chimica Acta.*, **2001**, *441*(2), 257–268. https://doi.org/10.1016/S0003-2670(01)01114X

Ghimire, K. N. Functionalization of orange waste with phosphoric group for Anion separation. *Journal of Nepal Chemical Society*, **2013**, *29*, 110–112. https://doi.org/10.3126/jncs.v29i0.9275

Giles, D. E., Mohapatra, M., Issa, T. B., Anand, S., & Singh, P. Iron and aluminium based adsorption strategies for removing arsenic from water. *Journal of Environmental Management*, **2011**, *92*(12), 3011–3022. https://doi.org/10.1016/j.jenvman.2011.07.018

Gnawali, C. L., Shahi, S., Manandhar, S., Shrestha, G. K., Adhikari, M. P., Rajbhandari, R., & Pokharel, B. P. Porous activated carbon materials from Triphala seed stones for high-performance supercapacitor applications. *Bibechana*, **2023**, *20*(1), 10–20. https://doi.org/10.3126/bibechana.v20i1.53432

Goourlot. *Application of methylene blue adsorption to cotton fiber specific surface area measurement: Part I methodology*, **1998**, *6*(11), *164–173*.

Gulens, J., & Anson, F. C. Characterization of the products resulting from electrochemical reduction of dichlorobis(ethylenediamine)rhodium$^{1+}$ at mercury electrodes (world). *ACS Publications; American Chemical Society*, **2002**, 5(7), 67-75. https://doi.org/10.1021/ic50129a016

Heitkemper, D. T., Vela, N. P., Stewart, K. R., & Westphal, C. S. Determination of total and speciated arsenic in rice by ion chromatography and inductively coupled plasma mass spectrometry. *Journal of Analytical Atomic Spectrometry*, **2001**, *16*(4), 299–306. https://doi.org/10.1039/b007241i

Ho, Y. S., & McKay, G. Pseudo-second order model for sorption processes. *Process Biochemistry*, **1999**, *34*(5), 451–465. https://doi.org/10.1016/S0032-9592(98)00112-5

Hu, S., Lu, J., & Jing, C. A novel colorimetric method for field arsenic speciation analysis. *Journal of Environmental Sciences*, **2012**, *24*(7), 1341–1346. https://doi.org/10.1016/S1001-0742(11)60922-4

Jha, P. K., & Jha, V. K. Arsenic Adsorption Characteristics of Adsorbent Prepared From Spinacia oleracea (Spinach) Leaves. *Scientific World*, **2021**, *14*(14), 51–61. https://doi.org/10.3126/sw.v14i14.34987

Jjagwe, J., Olupot, P. W., Menya, E., & Kalibbala, H. M. Synthesis and Application of Granular Activated Carbon from Biomass Waste Materials for Water Treatment: A Review. *Journal of Bioresources and Bioproducts*, **2021**, *6*(4), 292–322. https://doi.org/10.1016/j.jobab.2021.03.003

Jong, E. D. Comparison of three methods of measuring surface area of soils. *Canadian Journal of Soil Science*, **1999**, *79*(2), 345–351. https://doi.org/10.4141/S98-069

Kamsonlian, S., Balomajumder, C., & Chand, S. Removal of As (III) from Aqueous Solution by Biosorption onto Maize (Zea mays) Leaves Surface: Parameters Optimization, Sorption Isotherm, Kinetic and Thermodynamics Studies. 1.*Indian Journal*, **2012**, 5(7), 5-9.

Kanel, S. R., Das, T. K., Varma, R. S., Kurwadkar, S., Chakraborty, S., Joshi, T. P., Bezbaruah, A. N., & Nadagouda, M. N. Arsenic Contamination in Groundwater: Geochemical Basis of Treatment Technologies. *ACS Environmental Au.*, **2023**, *3*(3), 135–152. https://doi.org/10.1021/acsenvironau.2c00053

Karmacharya, M. S., Gupta, V. K., Tyagi, I., Agarwal, S., & Jha, V. K. Removal of As(III) and As(V) using rubber tire derived activated carbon modified with alumina composite. *Journal of Molecular Liquids*, **2016**, *216*, 836–844. https://doi.org/10.1016/j.molliq.2016.02.025

Kundu, R., Kunnoth, B., Pilli, S., Polisetty, V. R., & Tyagi, R. D. Biochar symbiosis in anaerobic digestion to enhance biogas production: A comprehensive review. *Journal of Environmental Management*, **2023**, *344*, 118743. https://doi.org/10.1016/j.jenvman.2023.118743

Kuriakose, S., Singh, T. S., & Pant, K. K. Adsorption of As(III) from Aqueous Solution onto Iron Oxide Impregnated Activated Alumina. *Water Quality Research Journal*, **2004**, *39*(3), 258–266. https://doi.org/10.2166/wqrj.2004.036

Lagergren, S. Ueber die Dämpfung electrischer Resonatoren. *Annalen Der Physik*, **1898**, *300*(2), 290–314. https://doi.org/10.1002/andp.18983000208

Langmuir, I. The adsorption of gases on plane surfaces of glass, mica and platinum. *Journal of the American Chemical Society*, **1918**, *40*(9), 1361–1403. https://doi.org/10.1021/ja02242a004

Lenoble, V. Arsenite oxidation and arsenate determination by the molybdene blue method. *Talanta*, **2003**, *61*(3), 267–276. https://doi.org/10.1016/S00399140(03)00274-1

Leonard, S. S., Harris, G. K., & Shi, X. Metal-induced oxidative stress and signal transduction. *Free Radical Biology and Medicine*, **2004**, *37*(12), 1921–1942. https://doi.org/10.1016/j.freeradbiomed.2004.09.010

Maity, S., Nanda, S., & Sarkar, A. Colocasia esculenta stem as novel biosorbent for potentially toxic metals removal from aqueous system. *Environmental Science and Pollution Research*, **2021**, *28*(42), 58885–58901. https://doi.org/10.1007/s11356-021-13026-1

Matlock, M. M., Howerton, B. S., & Atwood, D. A. Chemical Precipitation of Lead from Lead Battery Recycling Plant Wastewater. *Industrial & Engineering Chemistry Research*, **2002**, *41*(6), 1579–1582. https://doi.org/10.1021/ie010800y

Mianowski, A., Owczarek, M., & Marecka, A. Surface Area of Activated Carbon Determined by the Iodine Adsorption Number. *Energy Sources, Part A: Recovery, Utilization, and Environmental Effects*, **2007**, *29*(9), 839–850. https://doi.org/10.1080/00908310500430901

Mohan, D., & Pittman, C. U. Arsenic removal from water/wastewater using adsorbents—A critical review. *Journal of Hazardous Materials*, **2007**, *142*(1–2), 1–53. https://doi.org/10.1016/j.jhazmat.2007.01.006

Morrison, G. M. P., Revitt, D. M., & Ellis, J. B. Metal Speciation in Separate Stormwater Systems. *Water Science and Technology*, **1990**, *22*(10–11), 53–60. https://doi.org/10.2166/wst.1990.0288

Muñoz, O., Vélez, D., & Montoro, R. Optimization of the solubilization, extraction and determination of inorganic arsenic [As(III) + As(V)] in seafood products by acid digestion, solvent extraction and hydride generation atomic absorption spectrometry. *The Analyst*, **1999**, *124*(4), 601–607. https://doi.org/10.1039/a809426h

Nikić, J., Agbaba, J., Watson, M. A., Tubić, A., Šolić, M., Maletić, S., & Dalmacija, B. Arsenic adsorption on Fe–Mn modified granular activated carbon (GAC–

FeMn): Batch and fixed-bed column studies. *Journal of Environmental Science and Health, Part A*, **2019**, *54*(3), 168–178. https://doi.org/10.1080/10934529.2018.1541375

Pant, D., Singh, A., Van Bogaert, G., Irving Olsen, S., Singh Nigam, P., Diels, L., & Vanbroekhoven, K. Bioelectrochemical systems (BES) for sustainable energy production and product recovery from organic wastes and industrial wastewaters. *RSC Adv.*, **2012**, *2*(4), 1248–1263. https://doi.org/10.1039/C1RA00839K

Rajbhandari, R., Shrestha, L. K., & Pradhananga, R. R. Preparation of Activated Carbon from Lapsi Seed Stone and its Application for the Removal of Arsenic from Water. *Journal of the Institute of Engineering*, **1970**, *8*(1–2), 211–218. https://doi.org/10.3126/jie.v8i1-2.5113

Ratnaike, R. N. Acute and chronic arsenic toxicity. *Postgraduate Medical Journal*, **2003**, *79*(933), 391–396. https://doi.org/10.1136/pmj.79.933.391

Saha, G. C., Hoque, Md. I. U., Miah, M. A. M., Holze, R., Chowdhury, D. A., Khandaker, S., & Chowdhury, S. Biosorptive removal of lead from aqueous solutions onto Taro (Colocasiaesculenta(L.) Schott) as a low cost bioadsorbent: Characterization, equilibria, kinetics and biosorption-mechanism studies. *Journal of Environmental Chemical Engineering*, **2017**, *5*(3), 2151–2162. https://doi.org/10.1016/j.jece.2017.04.013

Schiewer, S., & Balaria, A. Biosorption of $Pb^{2+}$ by original and protonated citrus peels: Equilibrium, kinetics, and mechanism. *Chemical Engineering Journal*, **2009**, *146*(2), 211–219. https://doi.org/10.1016/j.cej.2008.05.034

Sen, T. K. Adsorptive Removal of Dye (Methylene Blue) Organic Pollutant from Water by Pine Tree Leaf Biomass Adsorbent. *Processes*, **2023**, *11*(7), 1877. https://doi.org/10.3390/pr11071877

Smedley, P. L., & Kinniburgh, D. G. A review of the source, behaviour and distribution of arsenic in natural waters. *Applied Geochemistry*, **2002**, *17*(5), 517–568. https://doi.org/10.1016/s0883-2927(02)00018-5

Thakur, J. K., Thakur, R. K., Ramanathan, A., Kumar, M., & Singh, S. K. Arsenic Contamination of Groundwater in Nepal—An Overview. *Water*, **2010**, *3*(1), 1–20. https://doi.org/10.3390/w3010001

Thapa, S., & Pokhrel, M. R. Removal of As(III) from Aqueous Solution Using Fe(III) Loaded Pomegranate Waste. *Journal of Nepal Chemical Society*, **2013**, *30*, 29–36. https://doi.org/10.3126/jncs.v30i0.9332

Thathong, V., Tantamsapya, N., Yossapol, C., Liao, C.-H., Wirojanagud, W., & Padungthon, S. Role of Colocasia esculenta L. schott in arsenic removal by a pilot-scale constructed wetland filled with laterite soil. *Heliyon*, **2019**, *5*(2), e01233. https://doi.org/10.1016/j.heliyon.2019.e01233

Wang, J.-K., & Higa, S. (Eds.). *Taro, a review of colocasia esculenta and its potentials*. University of Hawaii Press, **1983**, Vol.1, p456.

Wilde, E. W., & Benemann, J. R. Bioremoval of heavy metals by the use of microalgae. *Biotechnology Advances*, **1993**, *11*(4), 781–812. https://doi.org/10.1016/0734-9750(93)90003-6

World Health Organization. *A global overview of national regulations and standards for drinking-water quality*. World Health Organization, **2018**, Vol. 3, p5. https://apps.who.int/iris/handle/10665/272345

Yeo, K. F. H., Li, C., Zhang, H., Chen, J., Wang, W., & Dong, Y. Arsenic Removal from Contaminated Water Using Natural Adsorbents: A Review. *Coatings*, **2021**, *11*(11), 1407. https://doi.org/10.3390/coatings11111407

Zhu, J., Baig, S. A., Sheng, T., Lou, Z., Wang, Z., & Xu, X. Fe3O4 and MnO2 assembled on honeycomb briquette cinders (HBC) for arsenic removal from aqueous solutions. *Journal of Hazardous Materials*, **2015**, *286*, 220–228. https://doi.org/10.1016/j.jhazmat.2015.01.004

# APPENDIX

## 3.2 Determination of $\lambda_{max.}$ for Methylene Blue Solution

| Wavelength (nm) | Absorbance |
|---|---|
| 600 | 0.511 |
| 610 | 0.620 |
| 620 | 0.631 |
| 630 | 0.662 |
| 640 | 0.771 |
| 650 | 0.932 |
| 660 | 1.061 |
| 665 | 1.171 |
| 670 | 0.990 |
| 680 | 0.760 |
| 690 | 0.540 |

## 3.3 Calibration Curve of the Methylene Blue Solution

| Concentration(mg/L) | Absorption |
|---|---|
| 0.0 | 0.00708 |
| 1.0 | 0.26546 |
| 2.0 | 0.50494 |
| 3.0 | 0.64359 |
| 4.0 | 0.90197 |
| 5.0 | 1.04062 |
| 6.0 | 1.51169 |
| 7.0 | 1.71336 |
| 8.0 | 1.80632 |
| 9.0 | 2.08361 |
| 10.0 | 2.32308 |

## 3.4 Specific Surface Area Determination

### a. A plot of $C_e/Q_e$ versus $C_e$ of ACS

| Equilibrium Concentration, $C_e$ (mg/L) | $Q_e$ (mg/g) | $C_e/Q_e$ (g/L) |
|---|---|---|
| 0 | 0 | 0 |
| 13.196 | 219.93 | 0.06 |
| 47.368 | 205.95 | 0.23 |
| 69.366 | 150.80 | 0.34 |
| 94.995 | 206.51 | 0.46 |

### b. A plot of $C_e/Q_e$ versus $C_e$ of ACL

| Equilibrium Concentration, $C_e$ (mg/L) | $Q_e$ (mg/g) | $C_e/Q_e$ (g/L) |
|---|---|---|
| 0 | 0 | 0 |
| 28.086 | 401.23 | 0.07 |
| 46.425 | 273.08 | 0.17 |
| 56.713 | 162.04 | 0.25 |
| 68.564 | 195.89 | 0.35 |

### c. A plot of $C_e/Q_e$ versus $C_e$ of ACR

| Equilibrium Concentration, $C_e$ (mg/L) | $Q_e$ (mg/g) | $C_e/Q_e$ (g/L) |
|---|---|---|
| 0 | 0 | 0 |
| 13.196 | 164.95 | 0.08 |
| 37.722 | 314.35 | 0.12 |
| 55.449 | 291.84 | 0.19 |
| 78.852 | 281.61 | 0.28 |

### 3.5.1 Determination of $\lambda_{max.}$ of As (III) Solution

| Wavelength (nm) | Absorbance |
|---|---|
| 790 | 0.252 |
| 800 | 0.256 |
| 810 | 0.262 |
| 820 | 0.266 |
| 830 | 0.271 |
| 840 | 0.277 |
| 850 | 0.272 |
| 860 | 0.268 |
| 870 | 0.259 |
| 880 | 0.256 |

### 3.6.1 Calibration curves of As (III) ion solution

| Concentration(mg/L) | Absorption |
|---|---|
| 0.00 | 0.00 |
| 0.99 | 0.09 |
| 2.00 | 0.17 |
| 3.00 | 0.23 |
| 4.00 | 0.30 |
| 5.00 | 0.38 |
| 6.01 | 0.46 |

### 3.8 Batch Adsorption Isotherm Studies

| **Equilibrium Concentration, $C_e$ (mg/L)** | **$Q_e$** (mg/g) | **$C_e$ /$Q_e$ (g/L)** |
|---|---|---|
| 1.163 | 10.579 | 0.11 |
| 4.158 | 20.792 | 0.20 |
| 10.095 | 33.649 | 0.30 |
| 14.403 | 38.927 | 0.37 |
| 20.077 | 42.716 | 0.47 |
| 27.695 | 45.40 | 0.61 |
| 38.938 | 45.80 | 0.85 |
| 44.927 | 46.799 | 0.96 |
| 78.445 | 48.724 | 1.61 |
| 172.644 | 57.548 | 3.00 |

### 3.12: Desorption of As (III) using NaOH of different molar concentrations

| **Molar Concentration. of NaOH solution.** | **Conc. of As (III) inequilibrated filtrate(mg/L)** | **q (desorption) (mg/g)** | **% (Desorption)** |
|---|---|---|---|
| 0.05 | 9.18 | 3.06 | 15.11 |
| 0.1 | 33.07 | 11.02 | 54.43 |
| 0.5 | 39.51 | 13.17 | 65.03 |
| 1 | 51.14 | 17.04 | 84.18 |
| 2 | 56.02 | 18.67 | 92.21 |